The Planetary Science Journal, 5:172 (35pp), 2024 August https://doi.org/10.3847/PSJ/ad55f4

Comparing Rover and Helicopter Planetary Mission Architectures in a Mars Analog Setting in Iceland

Samantha Gwizd[1], Kathryn M. Stack[1], Raymond Francis[1], Fred Calef[1], Brett B. Carr[2], Chris Langley[3], Jamie Graff[4], Þorsteinn Hanning Kristinsson[5], Vilhjálmur Páll Thorarensen[5], Eiríkur Bernharðsson[5], Michael Phillips[2], Matthew Varnam[2], Nathan Hadland[2], Jahnavi Shah[4], Jeffrey Moersch[6], Udit Basu[6], Joana R. C. Voigt[1], and Christopher W. Hamilton[2]
[1] Jet Propulsion Laboratory, California Institute of Technology, 4800 Oak Grove Drive, Pasadena, CA 91011, USA; Samantha.j.gwizd@jpl.nasa.gov
[2] Lunar and Planetary Laboratory, University of Arizona, 1629 East University Boulevard, Tucson, AZ 85721, USA
[3] MDA, 9445 Airport Road, Brampton, ON L6S 4J3, Canada
[4] Institute for Earth and Space Exploration, Western University, Perth Drive, London, ON, Canada
[5] Department of Engineering, Reykjavik University, 102 Reykjavik, Iceland
[6] Department of Earth and Planetary Sciences, The University of Tennessee Knoxville, 1621 Cumberland Avenue, Knoxville, TN 37996, USA
Received 2024 February 13; revised 2024 May 28; accepted 2024 June 5; published 2024 August 7

Abstract

The Rover–Aerial Vehicle Exploration Network project field-tested planetary mission operations within a Mars analog environment in Iceland using stand-alone rover and helicopter architectures. Mission planning, implementation, and results are reported for the rover mission and briefly summarized for the helicopter mission. The outcomes of both missions are subsequently compared. Field implementation occurred from 2022 July to August at the Holuhraun lava flow. The rover science operations team executed a 14 sol (Martian day) mission that achieved mission, science, and sampling goals, including the contextualization, acquisition, and planned caching of two eolian and two rock samples. The helicopter science operations team executed a plan of comparable length but emphasized different science goals given long-range flight capabilities and landing limitations. The resolution and targetability of the rover payload enabled more detailed analyses, whereas the helicopter was better able to map flow-scale morphologies. The rover's exploration was limited by daily mobility duration limits and hazardous terrain, whereas the helicopter's exploration was constrained by landing site hazards. Resource limitations resulted from lengthier rover drives and data-volume-intensive helicopter imaging surveys. Future missions using combined rover–helicopter architectures should account for each spacecraft's resource needs and acknowledge system strengths in different geologic settings. Both missions served to establish operations strategies and mission outcomes to be applied to future combined rover and helicopter mission architectures, while the helicopter mission also evaluated strategies and outcomes for future stand-alone airborne missions. Findings in this work are relevant to future missions seeking to optimize strategies for planetary mission operations.

Unified Astronomy Thesaurus concepts: Rovers (1409); Mars (1007)

1. Introduction

Beginning with the Sojourner rover on the Pathfinder mission (The Rover Team 1997), robotic rover missions have provided paradigm-shifting perspectives of the Martian surface and revolutionized our understanding of Mars' geologic history (Golombek et al. 1999; Arvidson et al. 2006; Squyres et al. 2006; Farley et al. 2022; Vasavada 2022). Ground-based rover images have revealed evidence for diverse sedimentary processes and paleo-environmental conditions on Mars within lacustrine, fluvial, deltaic, and eolian deposits (Williams et al. 2013; Grotzinger et al. 2014, 2015; Stack et al. 2019; Mangold et al. 2021; Caravaca et al. 2022). Ground-based geochemical and mineralogical measurements have resolved composition down to grain and phenocryst scales (Rivera-Hernández et al. 2020; Farley et al. 2022; Udry et al. 2023), revealing complex rock-forming and alteration processes (McLennan et al. 2019; Rampe et al. 2020). Collectively, findings from rover-based studies support the hypothesis that Mars once hosted diverse aqueous environments and may have been habitable in the ancient geologic past (e.g., Arvidson et al. 2006; Grotzinger et al. 2014; Scheller et al. 2022).

Despite the considerable scientific return from rover missions, their exploration and mobility are limited by steep slopes, rocky terrain, and sand hazards. In contrast, unoccupied aircraft systems (UASs) can collect science observations over hazardous terrain that would not otherwise be accessible (James et al. 2020), but landing capabilities present their own limitations in hazardous terrain (Alibay et al. 2022). The successful deployment of the Ingenuity helicopter (a dual-rotor UAS) at Jezero crater (Alibay et al. 2022), having completed 72 flights during its mission, demonstrates the potential for helicopters (and other UASs) to increase the scientific return and rover planning capabilities of future missions that utilize both robotic systems (Golombek et al. 2022). Potential applications of helicopters, when paired with rovers, include (1) scouting sites for rover exploration, (2) imaging terrain and aiding in rover traverse planning, (3) improving rover and helicopter localization, (4) advance identification of high-priority science targets, (5) collecting and transporting scientific data and samples over hazardous terrain, and (6) providing broad geologic context for rover observations (Bapst et al. 2021). Helicopters also have great potential as a stand-alone mission design (Balaram et al. 2018; Barnes et al. 2021). Given the success of the Ingenuity helicopter on Mars and the planned

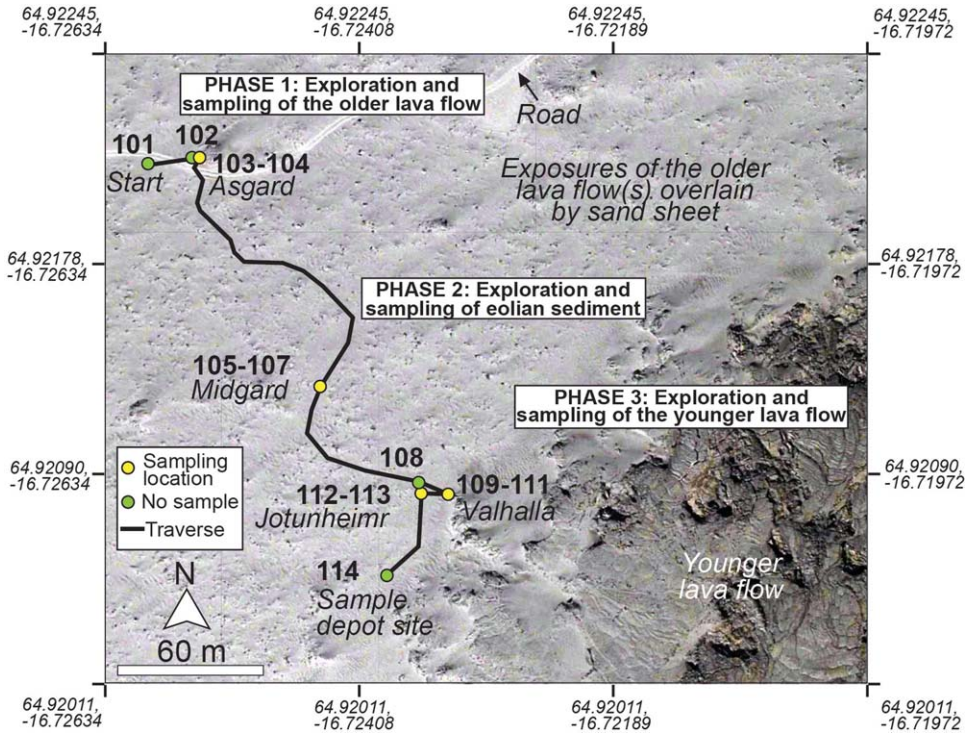

Figure 1. (a) Image showing the Holuhraun lava flow. The black box indicates the location in (b). The image is sourced from Loftmyndir Einkahlutafélag (50 cm pixel^{-1}). (b) Map of the 2022 rover traverse, showing the three mission phases and including remote science waypoints (green circles), sampling locations (yellow circles), and labeled sample names. The base map image is sourced from Scheidt & Hamilton (2019) and resampled to HiRISE resolution (25 cm pixel^{-1}).

future Dragonfly mission to Titan (Barnes et al. 2021), understanding how to use helicopters to increase the scientific return of future missions has never been more critical.

The aim of the Rover–Aerial Vehicle Exploration Network (RAVEN) project is to establish operational strategies to improve the scientific return of future rover–helicopter missions by conducting (1) separate rover and helicopter mission simulations to establish a baseline of individual mission capabilities and (2) a combined rover–helicopter mission. The mission simulations took place concurrently from 2022 July 22 to August 1 for the rover and 2022 July 25 to August 5 for the helicopter in the Holuhraun region of Iceland (Figure 1). The field site was selected because of its importance as a Mars analog terrain that exhibits similarities to large basaltic lava flows on Mars, including potentially habitable ancient environments (Voigt et al. 2021a; Duhamel et al. 2022; Hamilton et al. 2023). The primary rover mission objectives involved carrying out a 14 sol (Martian day) mission to characterize sites for Mars 2020 Perseverance-like sample selection (Figure 2; Farley et al. 2020). Science goals for both the rover and helicopter missions were developed in accordance with the goals of the Mars Exploration Program Analysis Group (MEPAG 2020) and primarily involved assessment of volcanogenic and eolian processes with implications for habitability.

This paper details the planning, implementation, and results of the 2022 RAVEN rover mission and compares the scientific, sampling, and mission results to the 2022 helicopter mission (Carr et al. 2024). Data and interpretations regarding science operations and sampling strategies, use of mission resources such as power and data volume, and overall scientific return from the 2022 field season will provide a basis from which to develop and implement a combined RAVEN rover–helicopter mission and help inform future single-vehicle mission development. Understanding the strengths and capabilities of each mission framework in a Mars analog environment ultimately helps to inform future strategies for conducting remote mission operations using rover, helicopter, and combined rover–helicopter architectures, objectives, and instrumentation.

2. Field Site

The Holuhraun region, located in the central Icelandic highlands, was chosen as the field site for the individual RAVEN rover and helicopter missions because of its geologic analogs to Mars (Hamilton et al. 2023). The primary feature in this region is the 2014–2015 Holuhraun flow (Figure 1(a)), formed from a reactivated fissure segment, last active in 1867 CE and associated with the Bárðarbunga–Veidivötn volcanic system (Bonnefoy et al. 2019). The main phase of this fissure eruption took place from 2014 August 31 through 2015 February 27 (Gudmundsson et al. 2016; Pedersen et al. 2017) and extruded a dense-rock equivalent volume of 1.21 km^3 (Bonny et al. 2018). The basaltic flow was emplaced over the Dyngjussandur flood plain as well as older basaltic lava flows (Figure 1(a); Hartley & Thordarson 2013). The 2014–2015 eruption emplaced lava into tributaries of the Jökulsá á Fjöllum river, resulting in the development of lava-heated springs (Bonnefoy et al. 2019; Dundas et al. 2020) that provided habitable environments for microbial communities (Duhamel et al. 2022).

Holuhraun was chosen due to its relevance as a high-fidelity Mars analog field site (Hamilton et al. 2023). Five of the key reasons for the site selection are as follows. (1) The location of Holuhraun in the central highlands of Iceland, at elevations greater than 600 m above mean sea level, is a barren region

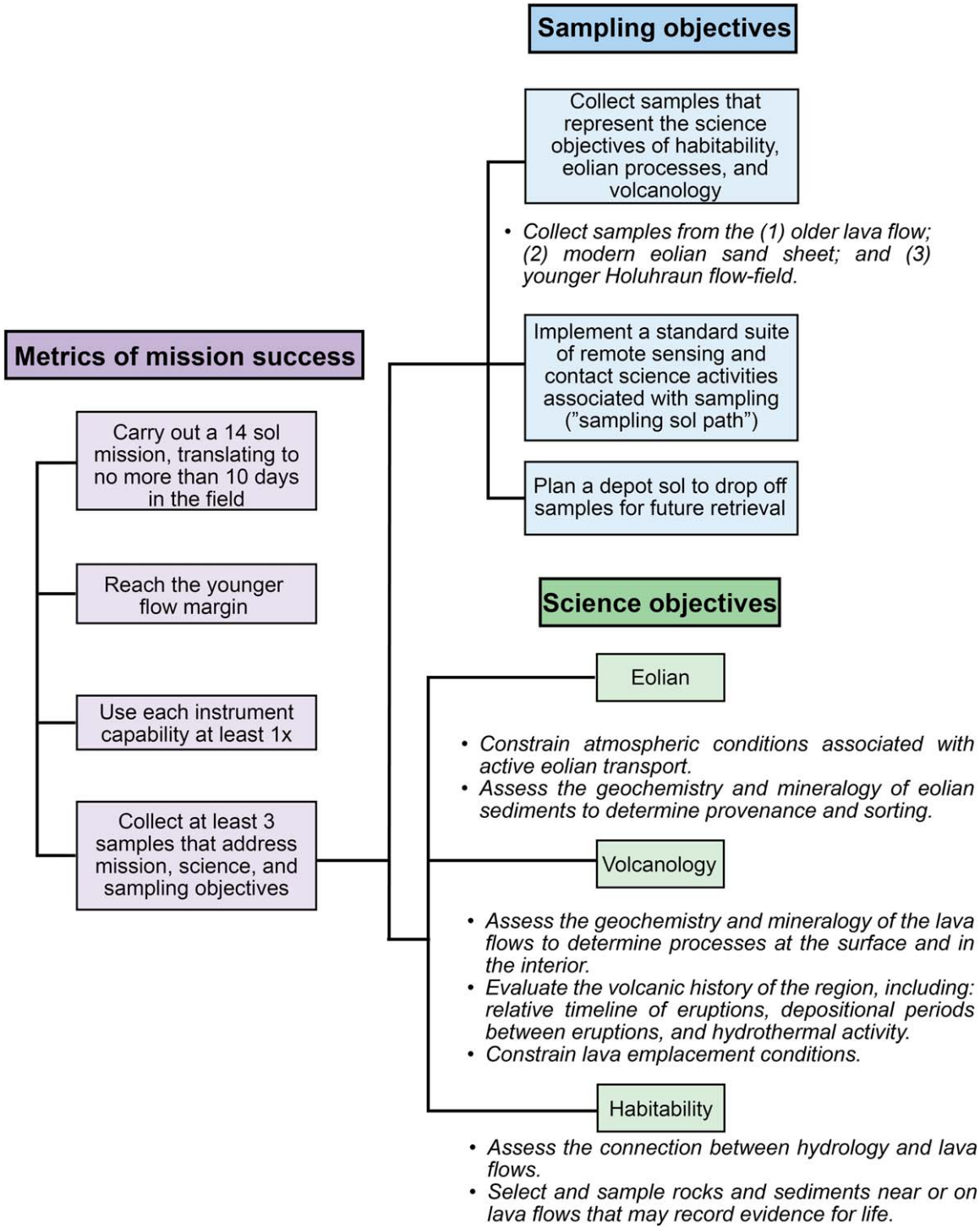

Figure 2. Chart showing mission, sampling, and science objectives.

with little vegetation cover other than isolated moss and lichen. (2) The region is predominantly composed of volcanic terrains that have been modified by eolian and glacial processes as well as glacial meltwater and catastrophic floods, thereby generating a Mars-like environment that includes a succession of lava flows emplaced within an active sand sheet. (3) Transitional lava flow types within the 2014–2015 Holuhraun lava flow exhibit similar morphologies to those observed on Mars (e.g., Elysium Planitia; Voigt et al. 2023) and may therefore inform aspects of their emplacement processes (Voigt et al. 2021a). (4) The emplacement of lava over a water-bearing glacial outwash plain resulted in development of habitable ephemeral hydrothermal systems that serve as an analog for assessing the astrobiological importance of lava–water interactions on Mars (Duhamel et al. 2022). (5) The region is accessible by road, with infrastructure available at the adjacent Askja central volcano, near Drekagil.

3. RAVEN Mission Objectives

The primary goals of the 2022 rover and helicopter missions were to acquire data and samples in a study area (Figure 1) that

would address the mission's science goals. The science goals of the 2022 RAVEN Mars analog mission followed MEPAG (2020) science goals to (1) determine if Mars ever supported or still supports life, (2) understand the processes and history of climate on Mars, and (3) understand the origin and evolution of Mars as a geologic system. As specifically applied to the Holuhraun field site, these objectives guided the main mission goals to (1) constrain the history, style, and dynamics of volcanism represented by the lava flows; (2) determine the nature of the eolian processes and present-day environment that formed the sand sheet; and (3) assess the habitability of the region encountered by the rover traverse by searching for evidence of water–rock interaction (Figure 2).

Based on a preliminary analysis of visible-wavelength images and stereo-derived topography (sources in Voigt et al. 2021a), degraded to the scale of High Resolution Imaging Science Experiment (HiRISE; McEwen et al. 2007) images ($\sim$25 cm pixel^{-1} for images and $\sim$1 m pixel^{-1} for digital terrain models, DTMs), we identified two lava flows of different ages within the study area (Section 5.1; Hamilton et al. 2023). The mission objective was to assess the geologic context of and sample those two lava units, and the overlying sedimentary deposits, within a 14 sol mission timeline, which could be conducted within no more than 10 good-weather days in the field. This time constraint defined the mission simulation's strategic planning (Section 5) and allocation of instrument and rover resources toward scientific activities (e.g., images, compositional measurements) versus engineering activities (e.g., driving, sampling). The mission strategy mimicked that of Mars 2020 (Farley et al. 2020). Another technical goal of the two missions was to use each instrument capability at least once. All objectives are summarized in Figure 2.

The primary sampling objectives of the rover and helicopter missions were to acquire a sample cache that fulfilled the RAVEN science objectives of characterizing volcanology, eolian processes, and habitability (Figure 2). The cache was planned to include at least three samples representing (1) the older lava flow, (2) eolian sediment from the sand sheet, and (3) the younger Holuhraun lava flow, with at least one sample also containing possible evidence for life (e.g., alteration of primary minerals, precipitation of secondary minerals). Acquiring samples on different lava flows would address the science goal of understanding the volcanic history of the region in addition to the goals to assess composition and determine processes at the surface and interior. Acquiring at least one eolian sample would address the science goals of understanding the provenance, sorting, and atmospheric conditions associated with eolian transport. Finally, the prioritization of an astrobiologically significant sample would address the habitability goals of assessing the connection between hydrology and lava flows and assessing evidence for life.

For the rover mission, acquisition of each sample would involve a preplanned suite of supporting scientific observations adapted from the sampling sol paths utilized on the Mars Science Laboratory (MSL) and Mars 2020 rover missions (e.g., Vasavada 2022; Table 1 in Simon et al. 2023; Section 6.5). A single sol was bookkept for the deposition of the sample cache at the end of the 14 sol mission, although it is acknowledged that a single sol for the depositing of multiple samples is likely not realistic given the recent Mars 2020 timeline with the Three Forks sample depot (Verma et al. 2024).

4. RAVEN Mission Design

4.1. RAVEN Rover Payload

The RAVEN rover mission simulated a rover payload based on recent Mars rover missions MSL Curiosity and Mars 2020 Perseverance. The payload suite was selected to be representative of the typical instrumentation available on an MSL- or Perseverance-class Mars rover (Grotzinger et al. 2012; Farley et al. 2020) and to replicate the types and volume of data, scientific capabilities, and resource costs associated with these instruments to explore an environment on Mars (Table 1).

The RAVEN rover payload included mast-mounted color navigation cameras and mast-mounted science cameras with narrower fields of view that were comparable to the MSL and Mars 2020 Navigation Cameras (NavCams; Maki et al. 2012, 2020) and M34 and M100 Mast Cameras (MastCams; Bell et al. 2017, 2021). The mast payload also simulated a remote spectrometer suite with laser-induced breakdown spectrometer (LIBS) and reflectance visible and infrared (VisIR) modes, as well as a narrow-field telescopic context camera (called the Remote Micro-Imager, RMI), based on the Mars 2020 SuperCam instrument and elements of the Chemistry and Camera (ChemCam) instrument (Wiens et al. 2012; Maurice et al. 2021). For conciseness, we refer to all associated activities as SuperCam, given the use of VisIR reflectance spectroscopy in this study. The rover payload also simulated two instruments deployable by a robotic arm: an alpha-particle X-ray spectrometer (APXS, modeled on the MSL instrument; Gellert et al. 2015) and a context imager comparable to the MSL Mars Hand Lens Imager (MAHLI) camera or Mars 2020 Scanning Habitable Environments with Raman and Luminescence for Organics and Chemicals (SHERLOC) Wide Angle Topographic Sensor for Operations and eNgineering (WATSON) camera (Edgett et al. 2012; Bhartia et al. 2021). For conciseness, we refer to the MAHLI instrument for all associated activities, as the usage of the camera as a primary science tool in addition to supporting sampling-associated activities is more consistent with the usage of the MAHLI camera on MSL.

The rover payload described above was simulated with analogous tools in the field, including handheld and tripod-mounted cameras that simulated the various science cameras and field contact spectrometers that represented the remote sensing spectrometers. Notably, both the rover's LIBS and APXS elemental composition data were simulated with the field LIBS device, for practical and safety reasons. The Canadian Space Agency's Mars Exploration Science Rover (MESR; Langley et al. 2012) has a built-in high-resolution monocular imager that was used during the first half of the mission simulation, but it was replaced by a tripod-mounted monocular camera when inclement weather precluded the use of MESR during the second half of the field exercise. The MESR rover and analog payload instrumentation were operated by a field implementation team in response to communication of science activity requests from the remote science operations team (Section 6).

The rover also had the capability to abrade and collect rock and sediment samples, analogous to the sampling capabilities of the Perseverance rover (Moeller et al. 2021). Abrasion was simulated for the RAVEN mission using a handheld drill that produced an abraded patch on the surface of a rock that was several centimeters in diameter. Drilling and core collection

Table 1
List of Simulated Rover Instruments and Their MSL/M2020-comparable Instrument

MSL/M2020-comparable Instrument	Description	Citation	RAVEN 2022 Rover Instrument	RAVEN 2022 Helicopter Instrument
NavCam	Gray-scale/color images providing context for targeting and traverse planning; stereo capabilities	Maki et al. (2012, 2020)	MESR monocular imager and tripod-mounted monocular camera	…
MastCam/MastCam-Z	Color images used to identify and measure landscape-to-outcrop-scale features; stereo capabilities	Bell et al. (2017, 2021)	Tripod-mounted camera	Airborne imaging camera
MAHLI/WATSON	Color images used to identify and measure smaller-scale features (micrometer–centimeter)	Edgett et al. (2012); Bhartia et al. (2021)	Handheld camera	Fixed, downward-pointing camera mounted on underside of UAV body
ChemCam/SuperCam RMI	Gray-scale/color images that enhance the contrast of fine-scale features (micrometer–centimeter)	Wiens et al. (2012); Maurice et al. (2021)	Tripod-mounted camera	…
ChemCam/SuperCam LIBS	Laser ablation breakdown spectrometer: 500 μm spot size	Wiens et al. (2012); Maurice et al. (2021)	Field LIBS instrument	Field LIBS instrument
SuperCam VisIR	Visible spectrum wavelengths of 400–853 nm (gap between 465 and 537); infrared wavelength between 1.3 and 2.6 μm	Maurice et al. (2021)	Point image spectrometer	Point image spectrometer
APXS	Alpha-particle X-ray spectrometer: particle-induced X-ray emission and X-ray fluorescence	Gellert et al. (2015)	Field LIBS instrument	…

Note. Also listed are the instruments used for the helicopter mission.

was performed using the same handheld drill, although the part of the rock that was ultimately cored and collected was not necessarily the same target selected by the science operations team per an agreement with Vatnajökull National Park to minimize the visible modification of rock outcrops. Sampling of unconsolidated sediment in the field was performed using a hand spade.

4.2. RAVEN Helicopter Payload Summary

The RAVEN helicopter payload was modeled after proposals for the Mars Science Helicopter concept (Johnson et al. 2020), which builds off that of the Mars 2020 Ingenuity helicopter (Balaram et al. 2018). The helicopter instrument payload was designed to have comparable capabilities as the rover's mast-mounted payload, though we note that Mars helicopters are not currently capable of carrying such a payload (Johnson et al. 2020). The helicopter instruments included an airborne imaging camera with a single axis of mobility, a fixed-focus microimager camera, a LIBS, and a VisIR spectrometer (Table 1). The helicopter also had sampling and abrasion capabilities. The microimager (similar to MAHLI) camera, LIBS, and VisIR spectrometer were all mounted to point at the same location directly underneath the helicopter's frame where the sample apparatus would disturb the ground surface. The helicopter was thus only capable of using these instruments to acquire data for the surface on which it landed.

5. Strategic Planning

5.1. Prelanding Science Assessment of Field Site

Members of the Rover and helicopter science operations teams had minimal to no prior knowledge of the Holuhraun region and refrained from reading relevant contextual scientific publications or geologic maps of the study site. Their only information came from the examination of remote sensing data that were provided for the simulations at resolutions equal to that of the Mars Reconnaissance Orbiter Context camera (6 m pixel^{-1}; Malin et al. 2007) and HiRISE (25 cm pixel^{-1}; McEwen et al. 2007) images. This process ensured that the science operations team's initial knowledge was comparable with that of a real mission scenario prior to landing at a new location on the surface of Mars.

The science operations teams used HiRISE-equivalent DTMs (1 m pixel^{-1}; Sutton et al. 2022) to establish regions of interest for the rover traverse and helicopter flights. From these data, the team differentiated three primary geologic units within the field site that formed the basis for strategic science mission planning (Figure 1): (1) an older lava flow surface underlying the sand sheet, (2) the overlying sand sheet, and (3) a younger flow overlying the older lava flow. Exposures of the older lava flow were more sparsely distributed compared to the contiguous, higher-standing younger lava flow, which the team hypothesized could be due to the substantial sand cover by the sand sheet. The team identified meter-scale eolian bedforms pervasive within the sand sheet. Variable textures were noted on the younger lava flow and appeared to generally correlate with distance from the flow margin, indicating that the textures could represent volcanic emplacement processes. The relative ages of the lava flows were inferred from superpositional relationships.

Of note, the science results presented in this paper originate exclusively from premission observations of remote sensing data and additional observations collected during the simulated mission campaign. As such, some interpretations may differ from established knowledge in the scientific literature based on more robust data sets. For instance, the rover- and UAS-based hyperspectral/geochemical measurements obtained in the field do not provide rare-Earth element and trace element information, but an effort has been made to draw general conclusions from the available data to highlight the value and limitations of comparable measurements on Mars.

5.2. Starting Site Selection and Strategic Plan Development

Whereas a Mars rover will land in a defined ellipse of several to tens of km in diameter (e.g., Dutta & Way 2017), typically some distance away from the first planned scientific campaign, the RAVEN team assumed the rover would have already driven to and arrived at its first waypoint of interest by the start of the mission in order to achieve mission goals within the allotted timeline. Adapted from landing site selection processes for Mars rover and lander missions (Golombek et al. 2012; Grant et al. 2018), the RAVEN science operations teams conducted "starting" site selection discussions beginning in the fall of 2021 (Basu et al. 2022), and the team met remotely to finalize a starting site and notional traverse path at a workshop in 2022 April. Criteria for starting site selection within the field area involved several scientific, logistical, and engineering constraints. A main constraint was that the rover starting site must provide the opportunity for mission and sampling objectives to be achieved within the timeline of the mission. To meet these objectives, the team determined that the rover had to be located less than ~350 m from the margin of the younger lava flow to account for the drive speed and distance and at a location where sand accumulation along the flow margin that might hinder the rover's access was minimal. Additionally, the RAVEN team chose to use the same starting site for both the rover and helicopter missions to enable more direct comparisons of mission metrics and of the rover traverse region using both missions' payloads. Logistically, the starting site had to be located proximal to an access road to enable delivery of the MESR rover. Engineering constraints were informed by MESR traverse capabilities. The maximum traversable slope by the rover with autonomous navigation is 28°, and the traverse speed is reduced when driving on sloped terrain (Langley et al. 2012). Therefore, to meet mission objectives and avoid hazardous conditions, the site had to offer at least one route to the younger lava flow margin with slopes less than 10°, no obstacles exceeding 25 cm in height (Langley et al. 2012), and that avoided regions of present-day, active flooding. The helicopter's landing pad requirements included a maximum 5° slope.

From the above criteria, a starting site and strategic plan were proposed for the rover that fulfilled the overall mission objectives as well as science and sampling objectives. The strategic traverse consisted of a total mission drive distance of ~200 m to reach the younger flow margin and subsequent depot site, with planned rover waypoints relevant to science and sampling goals (Figure 3(a)). The strategic path involved investigation of the older lava flow exposure(s) followed by the overlying sand sheet and the younger lava flow margin before driving to the sample depot site (Figure 3(b)). The first sample would be acquired at the exposure of the older lava flow shown in Figure 3(b), the second sample would be acquired from the

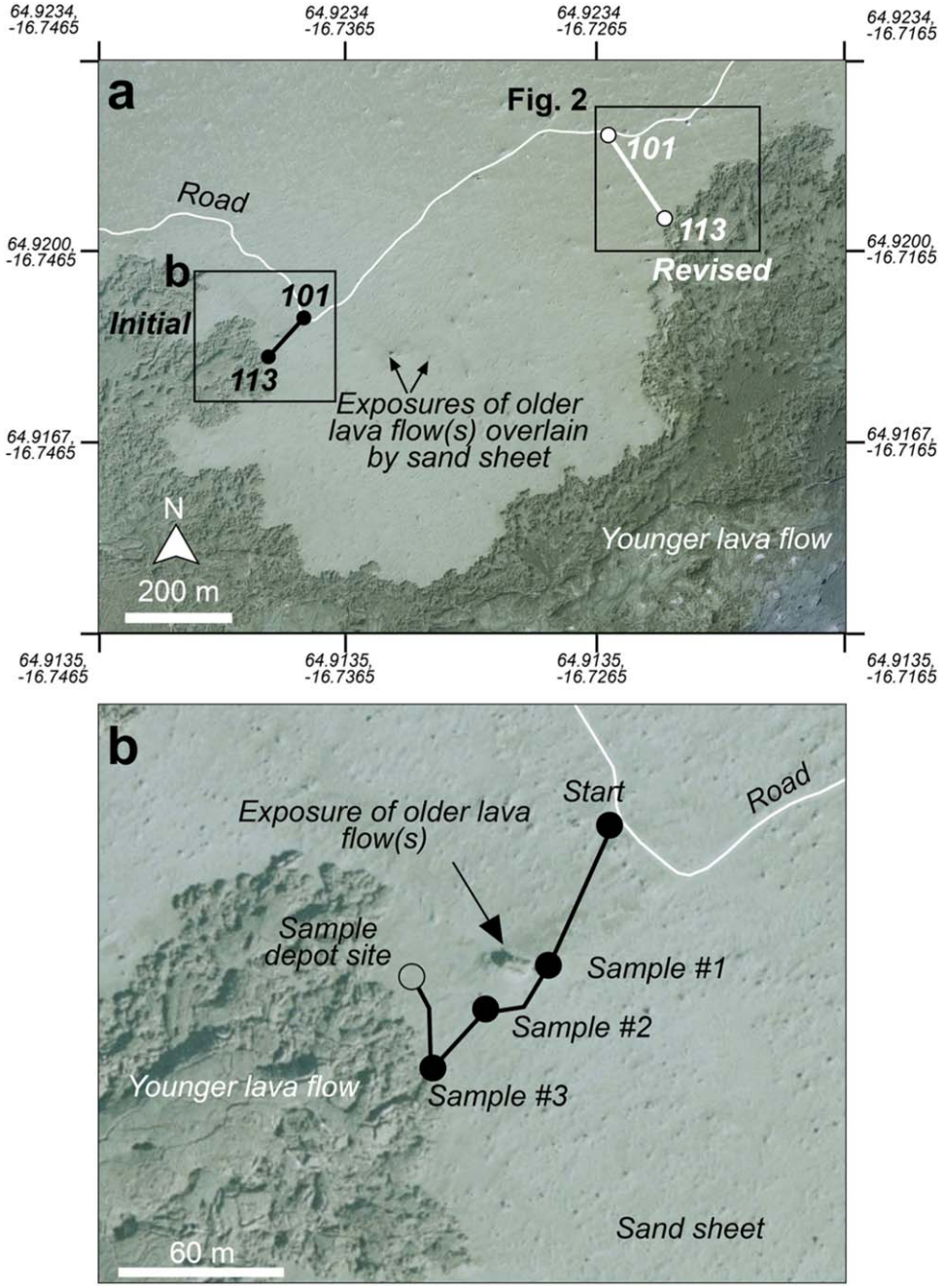

Figure 3. (a) Map depicting the initial rover traverse and the revised rover traverse. The initial rover traverse is shown in (b), and the revised rover traverse is shown in Figure 1(b). (b) Close-up view of the initial rover traverse. Both base maps are sourced from Loftmyndir Einkahlutafélag (50 cm pixel^{-1}).

sand sheet, and the third sample would be acquired from the younger lava flow margin.

5.3. Revised Starting Site

Upon arriving at the field area, the field implementation team discovered that the original selected starting site was inaccessible, so the rover and helicopter were deployed at a locality 675 m to the northeast of the original site that was still within the region of interest that was characterized to determine the preferred traverse route (Figure 1). The science operations teams chose the new mission starting point due to its ability to fulfill the same mission objectives as the original plan. The revised starting site was proximal to similar regions of interest to the initial site (Figure 1) and allowed for implementation of similar strategic plans (Sections 7.1–7.5) and fulfillment of the same mission objectives as the original plan. Differences in the revised traverse accounted for drive hazards and a greater overall drive distance to reach the younger flow margin (∼245 m).

5.4. Comparison of Rover and Helicopter Strategic Plans

Although the helicopter mission aimed to investigate the same three regions of interest as the rover (see Section 5.1), the helicopter science operations team prioritized scouting and flexibility over the identification of specific sampling targets and traverse paths in advance (Carr et al. 2024). The team's

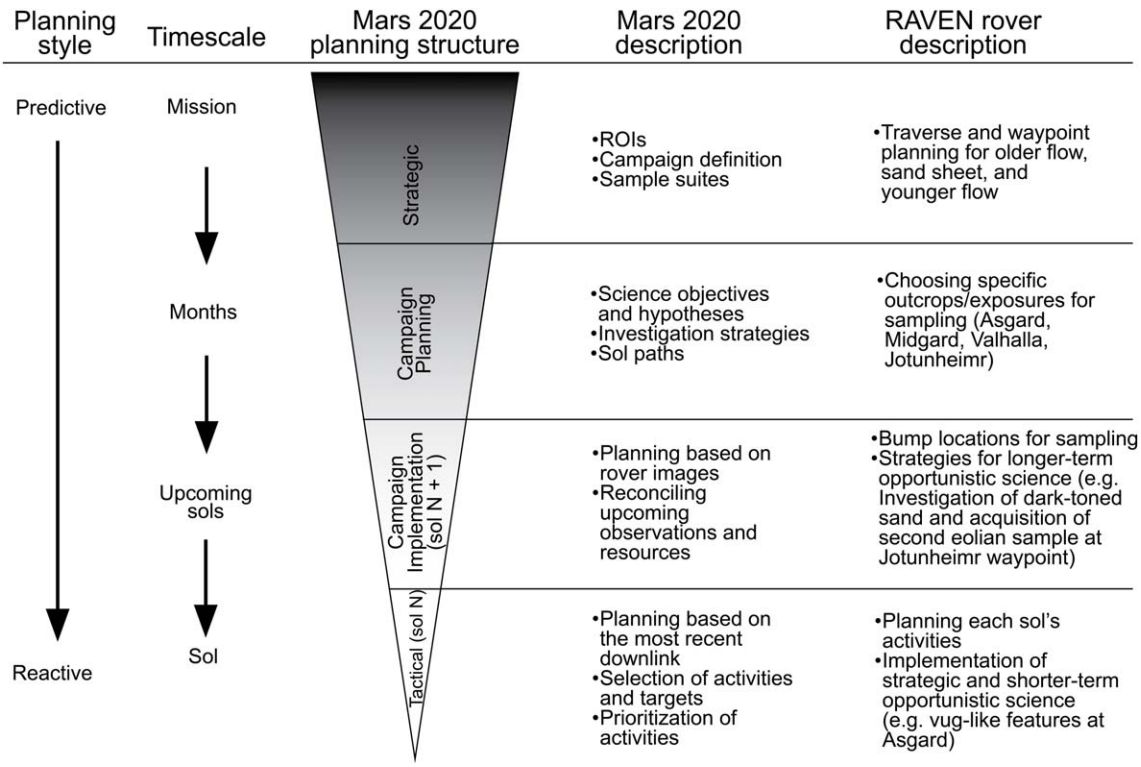

Figure 4. Schematic detailing the application of the Mars 2020 planning structure to the 2022 RAVEN rover mission.

approach was to identify areas of interest that could address the mission's science goals and then use reconnaissance flights to identify the best landing and sample sites in the area. Targets would then be prioritized on a sol-by-sol basis based on mission progress. The mobility of the helicopter compared with the rover enabled incorporation of more distal regions of interest on the younger flow into the strategic plan as well as a region of potential hydrologic significance that was beyond the scope of the rover mission timeline. To accommodate these more distant exploration targets, the helicopter science operations team deprioritized extended science investigations at any one site. While the rover starting site had to be accessible by the delivery truck, each sol's helicopter starting site needed to be accessible on foot by the field implementation team. This limited the helicopter from flying far into the Holuhraun flow, as this area was impossible to traverse on foot, or more than ∼1 km from the access road, due to the time required to hike over difficult terrain. Starting sites also had to meet terrain roughness criteria (e.g., smooth with nearly flat slopes; Carr et al. 2024).

6. RAVEN Rover Science Operations Design and Implementation

6.1. Science Operations Concept

The structure of the rover science operations approximated mission operations conducted on the Mars Exploration Rover missions (Yingst et al. 2014), MSL (Vasavada 2022), and Mars 2020 (Milkovich et al. 2022). Like Mars rover missions, science planning for RAVEN involved both predictive (i.e., strategic, long-term planning prior to significant data downlink from the rover) and reactive (i.e., tactical planning in response to results downlinked from previous sols) planning (Figure 4; Chattopadhyay et al. 2014; Milkovich et al. 2022). Each level of planning was designed to occur over different timescales, either pre- or post-landing. Strategic planning was done prior to the mission to establish the geology of the field site and a notional mission starting point (analogous to real rover landing site selection processes) and to constrain the main features of interest for exploration during the mission simulation, including a notional sol path and sampling strategy (Sections 5.2–5.3). Following initial candidate mission site characterization and down-selection from three sites to one (Basu et al. 2022), detailed campaign planning for RAVEN began in 2022 April and concluded just prior to the mission simulation start in 2022 July. The HiRISE-equivalent images were used for campaign planning to choose optimal rock or sediment exposures for sampling, remote science (use of the rover's mast instruments), and contact science (use of the rover's arm instruments) at the main regions of interest. Campaign implementation and tactical planning occurred daily. Campaign implementation constituted preplanning of the activities in the following sol or sols (sol $N + 1$), often drawing from interpretations of recent rover images. This planning level involved discussion of strategies for longer-term opportunistic science in subsequent sols or for refinement of planned campaign strategies (e.g., choosing specific locations on rock or sediment exposures selected during campaign planning for sampling). As the most reactive planning style, tactical planning (sol N planning) involved refinement of the relevant $N + 1$ plan in response to the most recent downlinked data, selection of science activities and targets in NavCam images, and prioritization of activities and enabled implementation of strategic and shorter-term opportunistic science.

In addition to science observations, planning also involved engineering activities. Common engineering activities include powering instruments on and off, rover arm mobility, abrasion and sampling, and driving (Table 2). A detailed explanation of

Table 2
Science and Engineering Activities Utilized in the 2022 Rover Mission

Type	Activity	Duration (minutes)	Data Usage (kB)	Energy Usage (Wh)	Notes
Science	SuperCam LIBS 3 points	7	6000	6	
	SuperCam LIBS 5 points	12	10,000	10	
	SuperCam LIBS 10 points	20	20,000	20	
	SuperCam VisIR 3 points	7	6000	6	
	SuperCam VisIR 5 points	12	10,000	10	
	SuperCam VisIR 10 points	20	20,000	20	
	SuperCam RMI image	1	2000	2	
	AEGIS analysis	5	1000	2	
	NavCam panorama	25	20,000	25	
	MastCam mosaic—workspace PDI	8	27,000	14	
	MastCam image—clast survey	3	6000	4	
	MastCam mosaic—Z30	3	4500	4	One frame
	MastCam mosaic—Z100	3	4500	4	One frame
	APXS—daytime short 45 minutes	45	300	7	
	APXS—daytime medium 90 minutes	90	500	14	
	APXS—overnight 12 hr	60	1000	100	
	MAHLI single image	4	6000	4	
	MAHLI standard suite (25, 5, 2 cm standoff)	8	18,000	8	
	MAHLI mosaic	10	24,000	10	4 × 1 5 cm standoff mosaic
Engineering	Rover traverse—autonav drive	55	2000	40	10 m drive
	Rover traverse—directed drive	35	1000	40	10 m drive
	ChemCam power ON	10	90	4	
	ChemCam power OFF	4	10	1	
	HazCam front left	5	50	1	
	HazCam front right	5	50	1	
	HazCam rear	5	50	1	
	Arm—unstow	20	500	45	
	Arm—stow	20	500	45	
	Arm—move	10	500	30	
	Arm—place on target	10	500	20	
	Arm—instrument swap	10	200	15	
	Rock abrasion	90	500	100	
	Sample acquisition	120	500	255	

the daily operations schedule and of the specific science and engineering activities that were implemented in the RAVEN rover mission is included in Section 6.4.

6.2. Resource Constraints

The resource budget, including daily power, data volume, and duration constraints, for the RAVEN rover mission was approximated from typical constraints on MSL and Mars 2020. For real Mars rover missions, the power budget is dependent on the season (directly related to the amount of heating required for the sol's activities) and the state of charge of the rover, which is dependent on the energy required to execute the previous sol's or sols' activities. For the RAVEN rover mission, the same daily power budget of 400 watt-hours (Wh), which is in line with rover missions (Crisp et al. 2003), was used on all but one sol of the simulation. On the one sol that the rover finished in a power-negative state, the power budget for the subsequent sol was adjusted to compensate. Daily downlink on a real rover mission varies daily depending on the timing, positioning, and availability of orbiter overflights, and only a subset of the total downlink data volume for the day arrives on Earth "decisionally," or in time for planning of the next day's activities. For the RAVEN simulation, we assumed a constant daily downlink volume of 140,000 kB, which is possible on rover missions (Edwards et al. 2013). We also assumed that all data arrived decisionally. The 140,000 kB data volume limit was imposed to force daily activity tradeoffs; on a real rover mission, some instruments have their own data volume storage capabilities, and the volume of data acquired on a given day can exceed the daily downlink volume but still be downlinked at a later sol. To avoid the need for daily data volume management over the course of the short simulation, we imposed a realistic daily total downlink volume but not did not impose a separate decisional downlink volume. A daily duration limit of 360 minutes was imposed for all science and engineering activities within the plan, consistent with other rover missions (Gaines et al. 2016).

Resource values were attributed to each science activity and scaled with modified parameters (e.g., adding additional frames to an image mosaic). Engineering activities (e.g., drives, arm movement) were also assigned resource values and were factored into the total daily resource budget (Table 2). Limiting resources on a given sol for a Mars rover mission derive from the tactical and plan content, relay orbiter timings, relay orbiter data volumes, and the state of the rover's power source (Vasavada 2022), whereas the power-, data-volume-, and duration-limited sols on the RAVEN mission solely derived from the plan content.

6.3. Roles

Planning was done remotely, with each individual member of the rover science operations team calling in to a virtual

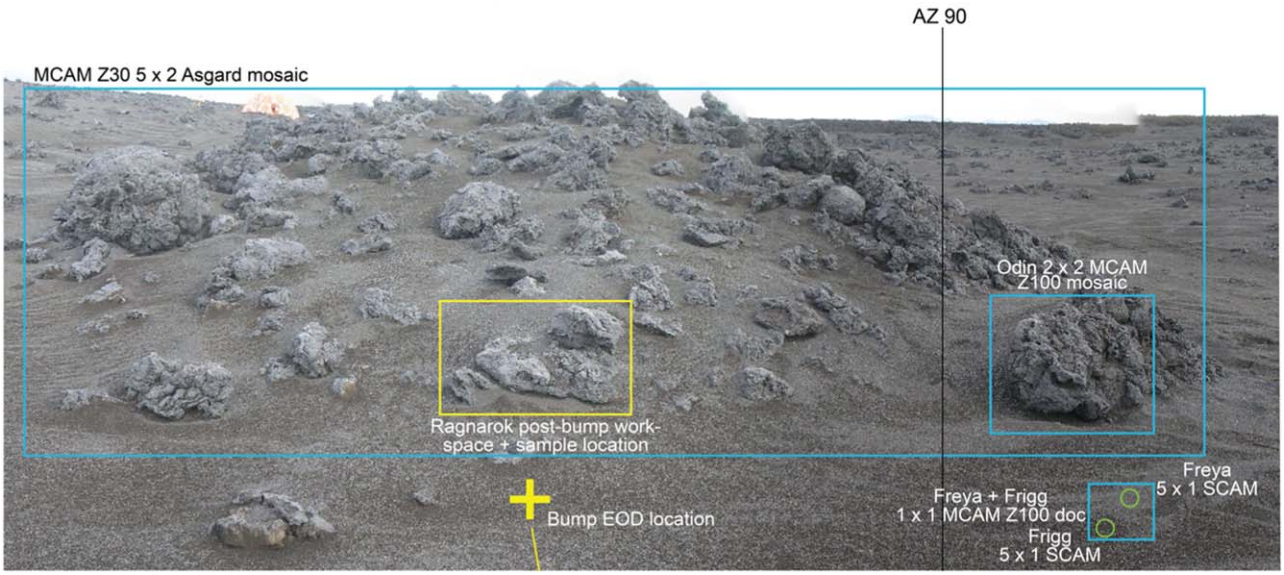

Figure 5. Example target map with labeled target names and corresponding activities from sol 102 tactical planning. MCAM = MastCam; SCAM = SuperCam; AZ = azimuth.

collaboration platform from their home institutions in the United States of America. Rover science operations roles were characteristic of roles on Mars rover missions but combined and/or modified for the RAVEN mission timeline, constraints, and personnel. Roles included the tactical science lead (TSL), science and rover planner (SARP), documentarian, and support scientist. The TSL facilitated daily remote operations meetings, leading discussions and providing final approval of the tactical ("N") plan. After planning concluded for the day, the TSL communicated the plan to the field implementation lead ("plan translation") in Iceland via phone call. The SARP selected activities in a planning spreadsheet and verified that the plan met resource constraints (see Section 6.2). The SARP also annotated NavCam and MastCam images with chosen activities for each sol's plan ("target maps"; Figure 5) and sketched out drive paths, including the end of drive location and orientation of the rover required for planning on the following sol. The documentarian produced reports for each planning day that detailed major planning decisions. Decisions included scientific observations and their intent for the tactical and handover plans as well as any scientific breakthroughs that resulted in operations-critical decisions. The support scientist provided preliminary interpretations of recent data to help contextualize and justify targets of interest within a workspace as well as at future locations. All participants generally participated in discussions of data interpretations and science objectives.

The field implementation team consisted of a field implementation lead and several technicians. The field implementation lead was in communication with the TSL to relay the uplinked plan and downlink data to the rover science operations team.

6.4. Planning Schedule

The rover science operations team followed a schedule that was slightly shortened relative to, but consistent with, a typical day of Mars rover planning. The daily schedule is depicted in Table 3. Each day began with a 1 hr period of data analysis, synthesis of downlinked data from a previous sol or sols, and presentation and report preparation. The start of operations involved a downlink assessment meeting to assess data received from the previous sol or sols and to discuss the implications of science interpretations for that day's planning. Following downlink assessment, the planning kickoff meeting entailed an overview of broad campaign goals and specific resource constraints (power, data volume, duration) to consider while planning the upcoming sol's science activities. Details regarding resource values utilized in the mission can be found in Section 6.2. During tactical planning, the team first verified the selection of a plan type suitable for the day's highest science and engineering priorities (e.g., long drive, remote sensing plus drive, contact science, abrasion, or sampling). These plans were constructed prior to the mission simulation and included a baseline set of activity templates suitable for that sol. Science and engineering activities used during the rover mission are listed in Table 2. The team then selected targets from the NavCam mosaic (Figure 5) and refined parameters (e.g., number of mosaic image frames) for science activities in the rover's current workspace. All targets were informally named following the rover science operations team's chosen theme of Norse mythology. After tactical planning, the team checked that all activities and their

Table 3
Daily Rover Science Operations Schedule

Time	Meeting
1:00 pm[a]	Optional prep time
2:00 pm	Start of RAVEN rover operations
2:00–2:10 pm	Downlink assessment
2:10–2:25 pm	Planning kickoff
2:25–4:00 pm	Tactical (sol *N*) planning
4:00–4:25 pm	Plan review
4:25–4:55 pm	Campaign implementation (sol $N + 1$) planning
4:55–5:00 pm	LAP
5:00–7:00 pm	Compilation of plan translation, report writing, LAP refinement, and margin

Note.
[a] All times listed above are PDT.

parameters were correct and that resource constraints were satisfied during plan review. Preplanning the following sol's activities occurred during campaign Implementation. The $N+1$ plan activities ranged in specificity depending on the plan type and anticipated location for the next sol. If the rover was anticipated to remain at the same workspace, a detailed $N+1$ plan, including target selection, could be constructed. If the rover was driving to a new location, template activities would be included in the plan, but targets and parameters were left unspecified. Finally, the look ahead planning (LAP) meeting included a brief discussion of the upcoming sol path (sol $N+2$ onward), including any possible action items that would arise in future planning several days later in the mission simulation. Upon conclusion of LAP, team members compiled reports and plan translation documents to transfer to the field implementation lead.

6.5. Realism

The science operations team had to reconcile the science goals of assessing habitability and biosignature preservation with the Icelandic terrestrial field site. Although the initial site selection process (Basu et al. 2022) avoided exploration zones that would be classified as "special regions" on Mars, referring to regions of specific water and temperature activity that may be contaminated by terrestrial organisms and may sustain extant Martian life (Olsson-Francis et al. 2023), the team was asked to be cautious of and ignore any such features during the mission. The team also ignored "Earth-isms" that would not exist on the Martian surface, including meteoric water and any vegetation (e.g., lichen).

The timeline of the mission simulation was highly condensed relative to a realistic Mars rover mission. Science campaigns on MSL and Mars 2020, particularly those involving sampling, typically have durations on the order of months to a year (Milkovich et al. 2022). The RAVEN mission simulation, including the collection of multiple samples, a series of long drives, and construction of a sample depot, condensed a likely months-long campaign in real rover operations into a 14 sol duration. One of the most time- and effort-intensive aspects of rover planning on Mars is the assessment of stereo data for traverse planning and the placement of the rover and rover's hardware relative to the surface of Mars during close-approach activities like contact science, abrasion, and sampling. Since stereo data were not a part of this simulation, the team carried out only a cursory assessment of mobility and outcrop hazards. However, the team attempted to select realistic drive paths with minimal hazards observed in "orbiter" images and selected outcrop targets for contact science, abrasion, and drilling that met similar size criteria as for MSL and Mars 2020 (i.e., targets with visible surfaces $\gtrsim$20 cm in diameter), with minimal obstructions for a theoretical rover arm.

A real rover mission experiences faults related to mobility, commanding errors, and exceedance of thermal or other operational limits, with the rate of faulting of Perseverance at $\sim$30% of all nominal sols (Sun et al. 2024). Given the limited duration of the mission simulation, the team decided against the introduction of unexpected faults that would prevent the mission simulation from achieving its science or operational objectives. As a result, all drives were successful and either met or exceeded the modeled and planned drive distance, and all activities executed as expected.

Table 4
Example Sampling Sol Path for Target Mjolnir

Sol	Activity	Description
103	Mastcam 5 × 3 mosaic	Documentation of workspace target Mjolnir
103	Abrasion	Abrasion of target Mjolnir
103	NavCam L	NavCam 1 × 1 for targeting
103	NavCam R	NavCam 1 × 1 for targeting
103	MAHLI standard suite	Abrasion of target Mjolnir
103	APXS 90 minutes	Abrasion of target Mjolnir
104	SuperCam LIBS/VisIR/RMI	Abrasion of target Mjolnir
104	Mastcam 1 × 1 Z100 Doc image	SuperCam target Mjolnir abrasion
104	Sample acquisition	Sample target Mjolnir
104	MAHLI 5 cm standoff	Mjolnir borehole

Multi-sol plans are typical for Mars rover missions due to weekend planning or when the Earth–Mars phasing falls outside of typical Earth working hours. However, certain activities, like the execution of contact science on an abrasion patch (Mars 2020), usually require ground-in-the-loop (i.e., the decisional downlink arrives on Earth prior to the planning of the day's activities) before the sol path can progress. However, several plans were constructed as 2 sol plans by the science operations team to enable the completion of 14 sols in no more than 10 working days in the field, thereby accepting that not all plans would be responsive to decisional downlink. The sampling activities incorporated a baseline sequence that combined concepts from MSL and Mars 2020 sampling sol paths: it was assumed that APXS (on the rover arm) could be placed on the abrasion patch without ground-in-the-loop (Table 4), similar to the relationship between the dust removal tool (Davis et al. 2012) and APXS on MSL (Vasavada 2022), whereas arm instruments on Mars 2020 typically require ground-in-the-loop following abrasion of a rock surface before placement (Simon et al. 2023).

Additionally, on the eighth sol of the mission simulation ($\sim$5 days into the field implementation), inclement weather hindered the field implementation team's ability to execute plans as originally expected. In response, the field implementation team acquired data for multiple plans within a single day when the weather cleared. The field implementation team lead is experienced in Mars rover science operations, and so the team was able to anticipate the targets and activities that the science operations team would be likely to request. Although the data acquired were largely similar to what would have been requested, the second half of the mission simulation was only partially able to capture the science operations team's realistic response to decisional downlink.

7. RAVEN Rover Mission Narrative

7.1. Overview

The rover mission simulation began on sol 101 while the rover was still positioned at its designated starting site (Section 5; Figures 1 and 3). Sol 101 was selected for the start of the mission under the assumption that commissioning activities typical of a newly landed rover on Mars had already been completed, and the rover was prepared to embark on its first science campaign with all science and engineering capabilities released. Given the geologic context of the field site and the existing strategic science plan, the science

operations team subdivided the mission into three main exploration phases: (1) older lava flow, (2) sand sheet, and (3) younger lava flow. For each of the mission phases, the notional sol path involved (1) a drive sol (>15 m) to reach the initial outcrop or eolian bedform where a suitable sampling site would be chosen, followed by postdrive imaging (PDI) comprised of a NavCam mosaic, a MastCam image of the targetable workspace, a MastCam clast survey (a systematic survey image of the ground after each drive; Yingst et al. 2013), and a SuperCam Autonomous Exploration for Gathering Increased Science (AEGIS) LIBS/VisIR activity (see Francis et al. 2017 for details regarding AEGIS); (2) a bump (minor reorientation in the rover position, <15 m short drive) sol to move the rover within sampling distance from the site; (3) a science sol where remote sensing (MastCam and SuperCam), contact science (MAHLI and APXS), and the option of rock abrasion would be used to investigate the sample site; and (4) a sampling sol (Tables 4 and 5). Following acquisition of three samples, one from each of the main geologic units described above, and with several sols remaining in the simulation, the team decided to collect a second sand sheet sample prior to the sample depot sol. Sol 113 involved a drive to a sample depot site, and sol 114 bookkept deposition of the sample cache at this site (Figure 1). The detailed list of all planned activities across the rover mission is included in Table A1.

7.2. Phase 1: Exploration of the Older Lava Flow (Starting Site to "Asgard," Sols 101–104)

The main goal of the rover's phase 1 exploration was to document the morphology and composition of the older lava flow. Initial observations of the older flow were acquired on sol 101 from the starting site (Figure 1) and included MastCam and SuperCam activities on two sub-meter-scale rocks. Subsequently, the rover traversed ∼18 m east to the outcrop "Asgard" (Figure 6(a)), chosen for its proximity to the starting site and higher topographic expression relative to the surrounding landscape. The science operations team interpreted the high standing nature of the exposure as indicative of a relatively more coherent outcrop compared to the sparsely distributed blocks in the vicinity of the starting site.

The sol 101 drive ended ∼5 m from the Asgard outcrop, affording the team a complete view of its western face in the postdrive NavCam mosaic. The team identified variable morphologies within the outcrop, including rounded boulder-sized clasts (yellow arrow in Figure 6(a)), but determined that the rocks at Asgard appeared otherwise homogeneous in terms of finer-scale textures (e.g., phenocrysts, vesicles). A decision was therefore made to abrade and sample a nearby rock ("Ragnarok"), which had a relatively flat surface ideal for coring. The sample target on Ragnarok was designated "Mjolnir" and chosen for the presence of millimeter-scale, mineralized veins (Figure 7(a)) that could be of potential astrobiological significance. The following sols (103–105) focused on abrasion and sample acquisition, with additional remote sensing and contact science to characterize the sample site as resources and time allowed.

In addition to the mineralized veins at the "Mjolnir" sample target, the team observed several features of potential astrobiological significance. Upon closer inspection in higher-resolution images, some outcrop surfaces exhibited a red hue (Figure 6(b)) and were targeted to assess potential alteration by water (e.g., oxidation). White circular features that were topographically distinct relative to the rock were identified and hypothesized to represent the products of secondary fluid flow (Figure 6(c)). These features exhibited various shapes, with some appearing more veinlike and some appearing vuggy. However, it was later determined that these vuggy features were lichen, and observations specifically targeting these features were subsequently disregarded.

At both the starting site and Asgard, observations were conducted on several eolian sediment targets (Figure 6(d)). Observations revealed the presence of two sediment populations: light-toned coarser-grained sediment that appeared to mantle a dark-toned finer-grained sediment substrate. These findings motivated the team to prioritize assessment of both sediment populations in phase 2 (Section 7.3).

7.3. Phase 2: Exploration and Sampling of Eolian Sediments ("Midgard," Sols 105–107)

After a 100 m drive, the rover stopped at "Midgard" to begin phase 2 of the mission (sols 106 and 107; Figures 1 and 8(a)). The main goal of phase 2 was to document the eolian bedforms, grain sizes, and compositions of the sand sheet that could be used to constrain active sediment transport and environmental conditions. The darker- and lighter-toned sediment populations observed near Asgard were also present at Midgard (Figure 8(b)) and formed the focus of phase 2 exploration.

The suite of science observations conducted at Midgard were generally similar to those of phase 1, involving a suite of remote and contact science activities, followed by sampling. Given that there were no rock targets to abrade at this site, and the sampling target decision was relatively straightforward given the options available in the workspace, the team was able to condense contact science and sampling to fit on a single sol. To further constrain the relationship between the light and the dark sediment, the science operations team decided to simulate a wheel scuff, a technique used with Mars rovers in which one of the rover's wheels is used to disturb a sediment deposit and reveal a cross-sectional view of the stratigraphy (Sullivan et al. 2011). Imaging of the disturbed sediment allowed the team to see the mantling relationship of the light-toned coarser-grained sediment overlying the dark-toned finer-grained sediment (Figure 8(c)).

The team decided to prioritize sampling the light-toned sediment on a ripple target at Midgard (Njord; Figure 7(b)). During the sol 106–107 LAP meeting, the team decided to acquire a fourth opportunistic sample on the dark-toned sediment following the younger lava flow campaign of phase 3.

7.4. Phase 3: Approach to and Arrival at the Margin of the Younger Lava Flow (Valhalla, Sols 108–111)

The goal of phase 3 was to document the morphology and composition of the younger lava flow margin and acquire a sample of this lava at an accessible promontory called "Valhalla" (Figures 1(b) and 9(a)). Accessibility was a major factor in selecting a suitable outcrop for phase 3, as much of the younger flow margin is mantled by thick (∼2 m deep) sand ramps (Hamilton et al. 2023).

A 56 m drive south from Midgard placed the rover ∼15 m from the Valhalla exposure (sol 108 waypoint in Figure 1(b)). At the sol 108 waypoint, the rover science operations team conducted remote sensing activities on a nearby exposure of

Table 5
Rover Mission Sol Path

Planning Cycle	1	2	3	4		5		6		7		8		Not Planned
Sol	10	102	103	104	105	106	107	108	109	110	111	112	113	114
Location	RAVEN start site	Pre-Asgard	Asgard	Asgard	Asgard	Midgard	Midgard	Pre-Valhalla	Valhalla	Valhalla	Valhalla	Jotunheimr	Jotunheimr	Alfheim depot site
Main activities	Predrive RS, 18 m drive to Asgard, standard PDI	Predrive RS, ∼5 m bump to Asgard, standard PDI	RS, CS, and abrasion on Ragnarok block	Abraded science, coring Mjolnir	100 m autonav drive w/ mid-drive imaging, PDI	CS on eolian bedform, sampling of Njord	Predrive RS on bedforms, 56 m drive toward Valhalla, standard PDI	Predrive RS, 15 m bump, standard PDI	RS, CS, and abrasion on Yggdrasil block	RS on Fenrir abrasion, sampling Fenrir, CS on Fenrir borehole	Predrive RS, 11 m bump to Jotunheimr eolian site	CS on eolian sample (Valkyrie), sample Valkyrie	Predrive RS, 40 m drive toward depot site	N/A
Resource limitation	Data volume	Data volume	Energy	Energy	Duration	Energy	Duration	Data volume	Data volume	Energy	Data volume	Energy	Data volume	N/A

Note. RS = remote science; CS = contact science; PDI = postdrive imaging.

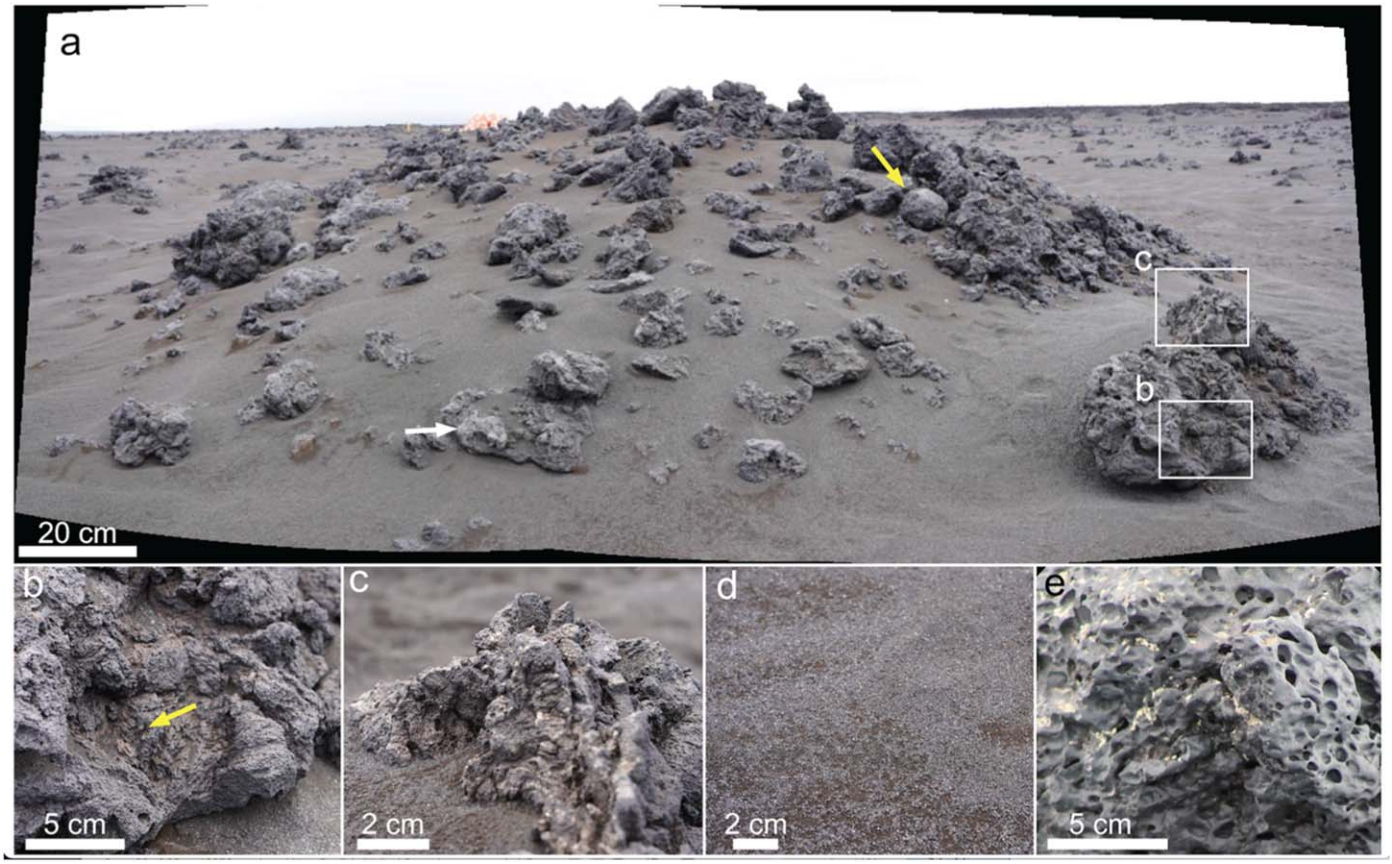

Figure 6. Representative phase 1 (sols 101–104) images captured at the Asgard site. (a) MastCam mosaic of the Asgard outcrop. The white arrow indicates the location of the sample Ragnarok. The yellow arrow indicates a possible rounded squeeze-out. White boxes correspond to the locations of (b) and (c). (b) Red hue (yellow arrow) showing evidence for alteration. (c) White circular features initially hypothesized to represent secondary fluid flow and targeted for their proposed astrobiological significance. (d) Representative image showing dark-toned and light-toned sediment populations at Asgard. (e) Representative millimeter- to centimeter-scale vesicles on the older lava flow.

rock (target Hel; Figure 9(b)) that appeared to have a similar morphologic and topographic expression to the older lava flow. Given that the rover was now 155 m away from Asgard, the team was motivated by a desire to assess lateral compositional variability within the older lava flow.

From the sol 108 position, the target "Fenrir" at the outcrop "Yggdrasil" was selected for sampling (Figure 7(c)), as the exposure appeared reachable by the rover arm and exhibited relatively flat surfaces suitable for drilling. Given preliminary assessments of Valhalla from the sol 108 NavCam images, there was no compelling evidence for significant heterogeneity (morphological or compositional) within the portion of the outcrop accessible to the rover, so the largest and most accessible target was selected.

After a 15 m bump, abrasion and sampling activities were conducted between sols 109 and 111 (Table 5). In addition to sample site characterization, the team prioritized remote sensing observations of other locations along the younger lava flow margin around Valhalla. Long-distance SuperCam RMI mosaics were planned on two margin exposures that exhibited unique morphologies observable in the NavCam PDI mosaic. One of the exposures, Nidavellir, is shown in Figure 9(c) and was thought to represent a lobe (Walker 2009; Hamilton et al. 2020).

7.5. Acquisition of a Second Eolian Sample (Sols 112–113)

During the sol 108 LAP meeting, when it became likely that there would be a few additional sols remaining after the acquisition of the younger flow sample, the rover science operations team discussed whether to sample a second eolian sample or a second sample on the younger lava flow margin at Valhalla. Several lines of reasoning supported prioritization of a second eolian sample. The "Njord" eolian sample collected at Midgard consisted predominantly of the light-toned, coarser-grained sediment population, but the dark-toned, finer-grained sediment population remained unsampled. In addition to the grain-size and tonal differences, VisIR data on a dark-toned target ("Niflheim"; Figure 10(a)) at the Midgard site showed absorptions at 1.4, 1.9, and 2.2 μm, consistent with hydration and hydrated silica (black arrows in Figure 10(a)), differentiating the dark-toned sediment population from the light-toned sediment population (Figure 10(b)) and of possible astrobiological interest. Furthermore, given the apparent lack of compositional or morphological diversity within the rocks at Valhalla and the limited accessibility of other sites along the flow margin, the team concluded that a second sediment sample, this time capturing the dark sediment population, would be higher priority than a second younger lava flow sample.

After an 11 m bump in the direction of the designated sample depot site (Figure 1), the sol 112–113 plan included standard sampling activities for the dark-toned sediment target "Valkyrie" (Figure 7(d)). Sample acquisition limited additional remote science activities, but the team was able to plan a mosaic on some nearby light-toned ripples. Following

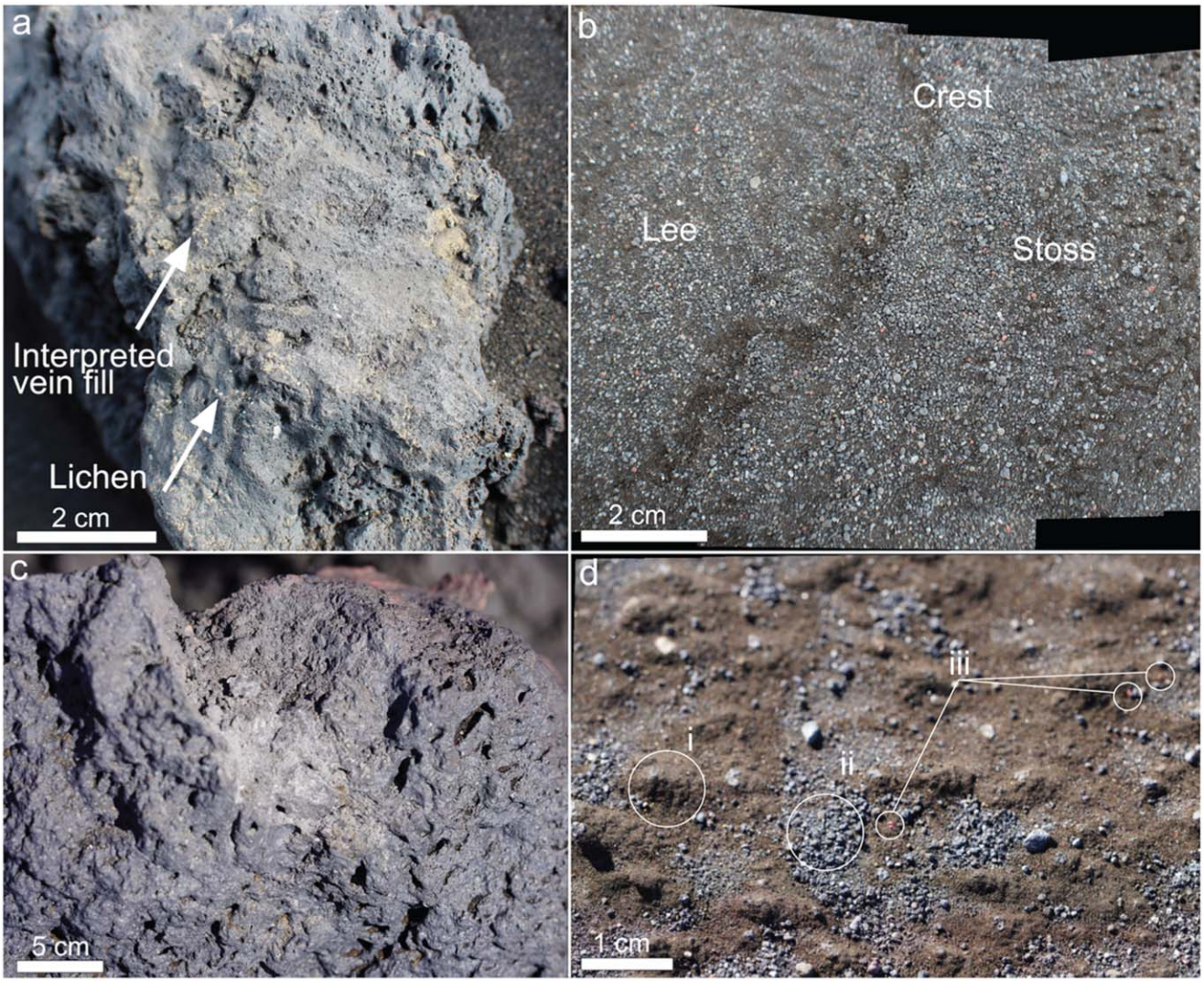

Figure 7. MAHLI images of rover sample targets, including (a) Ragnarok (older lava flow), (b) 4 × 1 mosaic of Njord (light-toned sediment), (c) Fenrir (younger lava flow), and (d) Valkyrie (dark-toned sediment). Annotations in (d) highlight key features in the sediment population: (i) indicates the dark-toned sediment population, (ii) indicates the light-toned sediment population, and (iii) indicates examples of scoria.

execution of the 112–113 plan, the team bookkept a drive to the sol 114 depot site "Alfheim" (Figure 1).

7.6. Summary of Rover Mission Metrics

The RAVEN rover mission simulation provides a basis by which to evaluate the science return and trade-offs between science and engineering. The following section summarizes the main metrics of the 2022 rover mission. Results are also shown in Table 6 and Figure 11.

The total distance traversed by the rover was approximately 245 m, with an average traverse distance on drive sols of 35 m. Traverse distances ranged from 5 m (bump to Asgard on sol 102) to ∼100 m (drive to Midgard on sol 105; Table 5). Drives were only planned on sols without abrasion or sampling activities, as is currently typical of the Mars 2020 mission. Drive sols were associated with duration- and data-volume-limited plans (Figure 11).

The team requested a total of 104 science observations (Table A1). Compositional measurements included 19 LIBS targets, 4 APXS targets (totaling 270 minutes), and 14 VisIR targets. Twenty-two compositional measurements were acquired on igneous rocks, and 15 measurements were acquired on the sand sheet. Energy usage of compositional measurements was relatively subequal between APXS, LIBS, and VisIR (Table A1). Image science activities consisted of 145 individual frames that captured 4 MAHLI targets, 26 MastCam targets, and 22 SuperCam RMI targets (Table A1). Twenty-seven image activities were acquired on igneous rocks, and 35 images were acquired on the sand sheet. The average data volume of image observations (11,061 kB) exceeded the data volume of compositional observations (7938 kB). Power usage was relatively equal between imaging and compositional observations, and neither category consumed significant power relative to driving, abrading, and samples (Table A1).

Resource limitations generally correlated with specific sol types. Data volume was the most common limitation for individual sol plans (Table 6). Six sols were limited by data volume. Of these six sols, five were characterized as "remote sensing and drive" sols (sols 101, 102, 108, 111, and 113; Table 5), and one was an abrasion sol (sol 109). Energy was the second most common limitation, with five sols limited by energy (sols 103, 104, 106, 110, and 112). All energy-limited sols involved abrasion or sampling activities (Figure 11). The

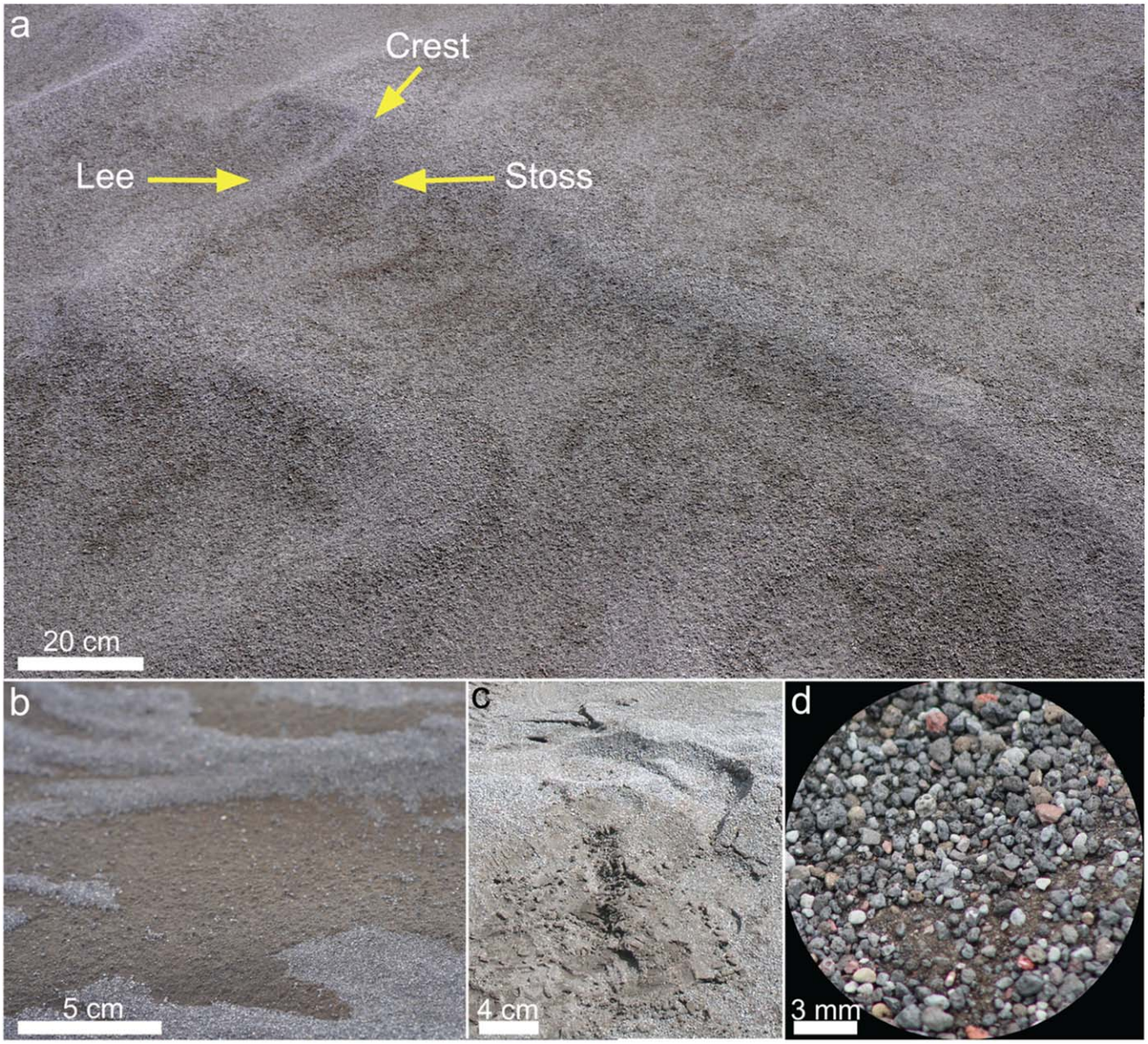

Figure 8. Representative phase 2 (sols 105–107) images captured at the Midgard site. (a) MastCam M100 of dark-toned sediment target Niflheim with overlying light-toned sediment. (b) Light-toned sediment and underlying dark-toned sediment. (c) Simulated wheel scuff, showing light-toned sediment and underlying dark-toned sediment. (d) RMI of light-toned sediment target Muspelheim, showing lithic grains.

sol 106 and 107 plan left the rover in a power-negative state that subsequently necessitated a relatively lower-power plan for sol 108. Finally, two targeted remote science and drive sols were limited by duration (sols 105 and 107).

7.7. Helicopter Mission Summary

The RAVEN helicopter mission was guided by the same mission, science, and sampling goals as the rover mission and involved a comparable instrument payload and mission duration (Carr et al. 2024). A visual summary of flight paths, landing sites, and sampling locations is depicted in Figure 12.

The helicopter mission shared the same mission starting site as the rover mission (sol 100; Figure 12). The shift in the mission starting location (Section 5.3) enabled the helicopter science operations team to assess a different sand sheet morphology with a smoother appearance and sparsely distributed light-toned boulders to the northeast of the starting site that was not part of the original strategic plan (sol 101 flight; Figure 12). Sol 102 involved a mapping survey of the area between the starting location and the younger lava flow margin, which included the entire rover mission traverse. A sediment sample was acquired near the flow margin on sol 103 (sol 102 landing site; Figure 12). The sample was carried with the helicopter during the sol 104 flight and deposited at the sol 104 landing location, which was designated by the helicopter team as the sample depot. The sol 104 plan involved a series of airborne images of the lava flow surface that the helicopter science operations team used to identify a location for a high-resolution mapping survey and a landing site on the younger lava flow. The survey and landing were executed on sol 105. Sols 106–108 involved acquisition of a lava flow sample and contact science on the flow surface at a location with a white

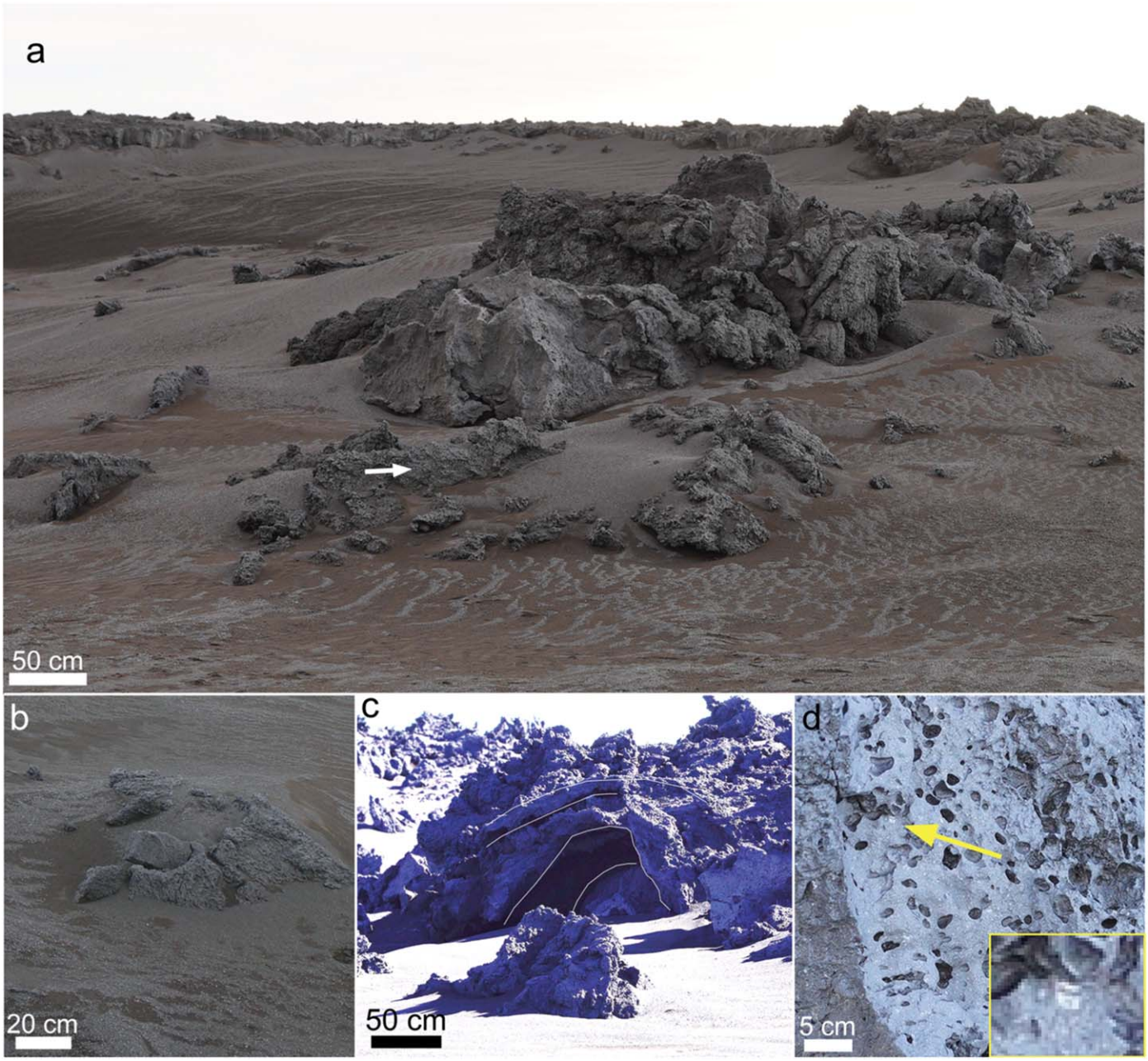

Figure 9. Representative phase 3 (108–111) images captured at the Valhalla site. (a) MastCam mosaic of the Valhalla promontory. The white arrow indicates the location of the sample Fenrir. (b) MastCam image of older lava flow target Hel. (c) MastCam image of Nidavellir, showing crust layers (white tracings). (d) Image of target Aegir showing millimeter-scale phenocrysts and millimeter–centimeter-scale vesicles. The yellow arrow indicates the location of the zoomed-in inset.

discoloration thought to represent alteration. The sol 109 plan involved collection of more airborne images of the lava flow and sand sheet while returning the lava sample to the depot location established on sol 104 (sol 104, 109, and 112 landing site in Figure 12). On sol 110, more images were acquired of the sand sheet followed by a landing on a flow margin breakout lobe identified from previous (sol 109) images. A sample from this flow lobe was taken on sol 111. Sol 112 involved acquisition of airborne images of lava textures on the younger flow located further west before returning to the sample depot to end the mission. Implementation of the sol 113 and sol 114 plans was not possible due to inclement weather.

The helicopter flew 10 km during a total of 29 minutes of flight time over nine flight sols. The helicopter returned 86 images to the science operations team, of which 51 were airborne oblique, 14 were taken at nadir during ascent or descent, 7 were horizontal images from ground level, and 7 were taken with the MAHLI camera of the ground surface beneath the helicopter while landed. Images from mapping survey flights (sols 101, 102, and 105) were postprocessed into digital elevation models (DEMs) and orthomosaics, covering a total area of 70,000 m^2 at a resolution of 30 cm $pixel^{-1}$ for the DEMs and 6–9 cm $pixel^{-1}$ for the orthomosaics. The LIBS and the VisIR point spectrometer each collected nine measurements from six different locations (each unique landing site), with before–after pairs from each sampling location. Three samples were cached, one of sand and two of the newer lava flow. The helicopter was not able to collect a sample or conduct any contact science on the older lava flow because these outcrops were too small and rough for the helicopter to land on, and the

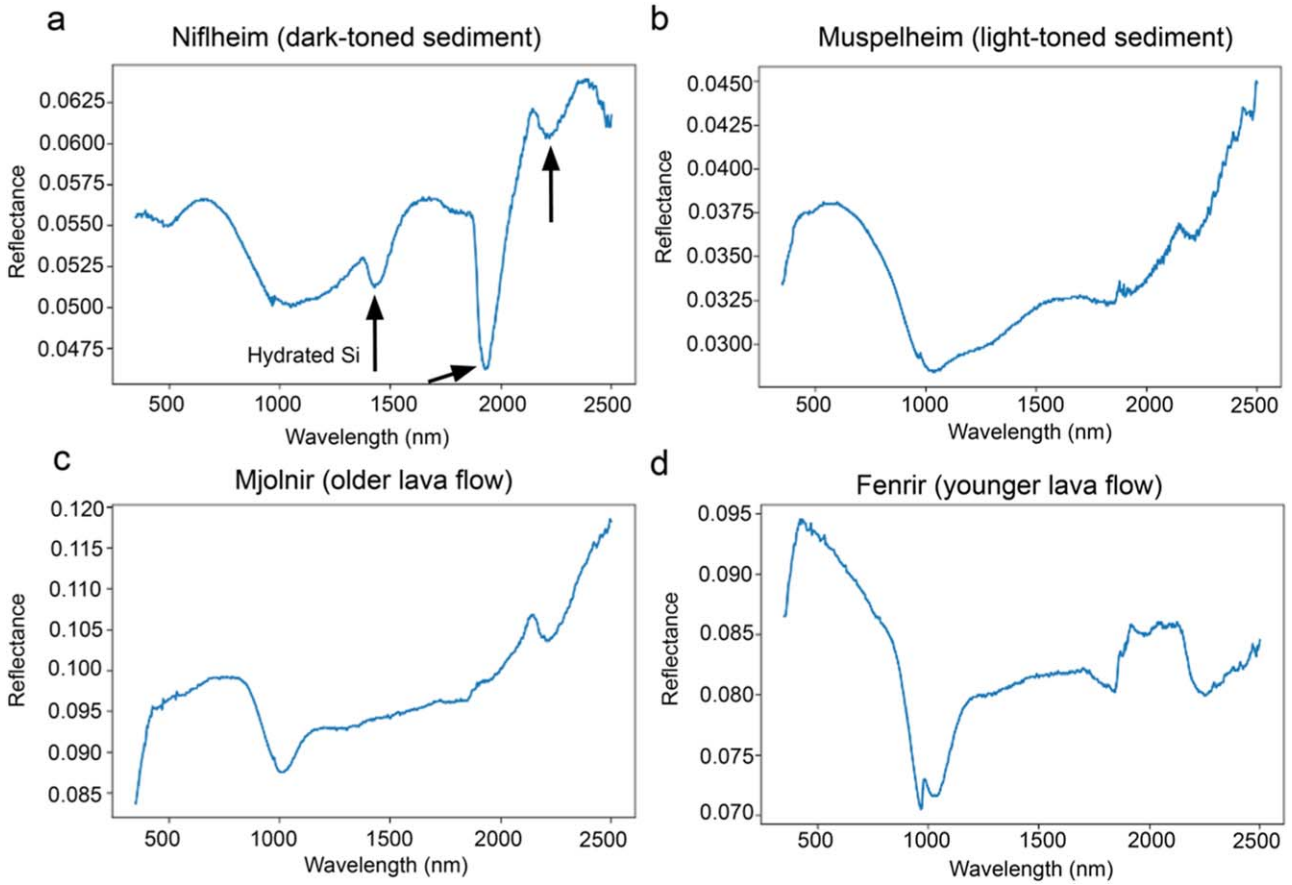

Figure 10. Representative VisIR plots showing (a) dark-toned sediment, (b) light-toned sediment, (c) older lava flow, and (d) younger lava flow targets. Black arrows in (a) show absorption features indicative of hydrated mineral phases.

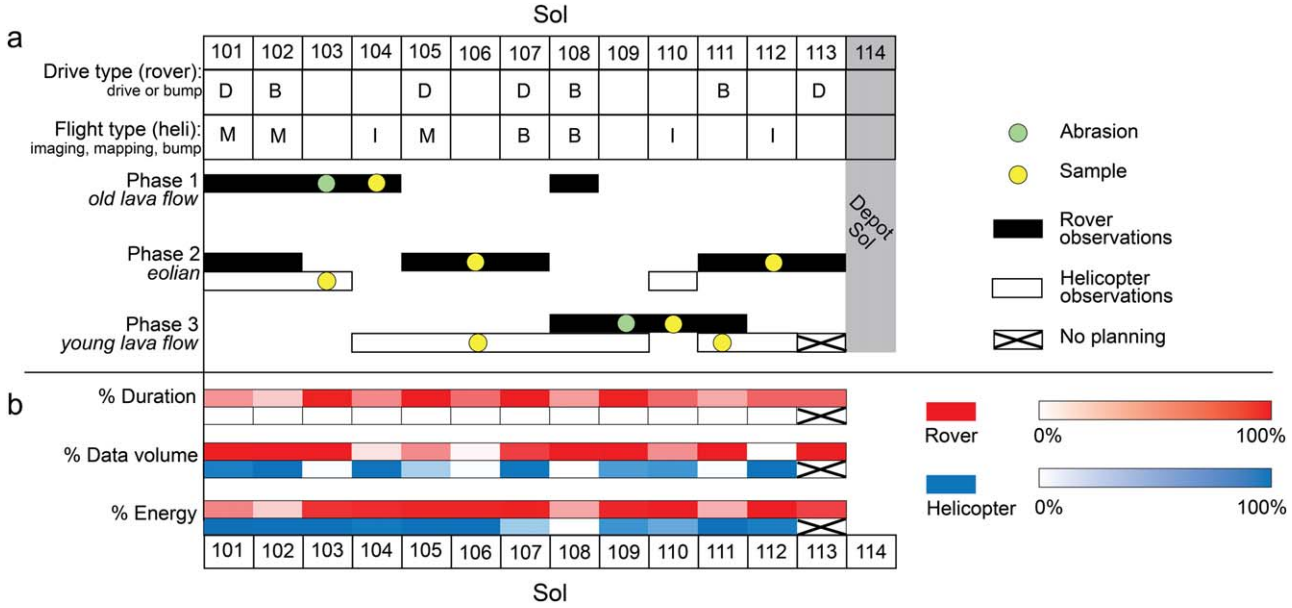

Figure 11. Comparison of the rover and helicopter missions. (a) Chart showing the distribution of each phase for the rover (black) and helicopter (white) missions. (b) Chart showing the allotment of resources for the rover (red) and helicopter (blue) missions. Tonal differences correspond to percentage values, which are also listed in Table 6.

system as designed was only able to conduct contact science activities at surfaces on which it had landed. The helicopter did, however, capture images of these outcrops from a few tens of meters away while airborne, allowing for some basic interpretations. The helicopter was able to land directly on the younger lava flow, performing contact measurements and sampling terrain otherwise inaccessible to the rover. The lava samples included rocks from a relatively smooth plateau ~200 m from the flow margin and from a breakout lobe at the margin.

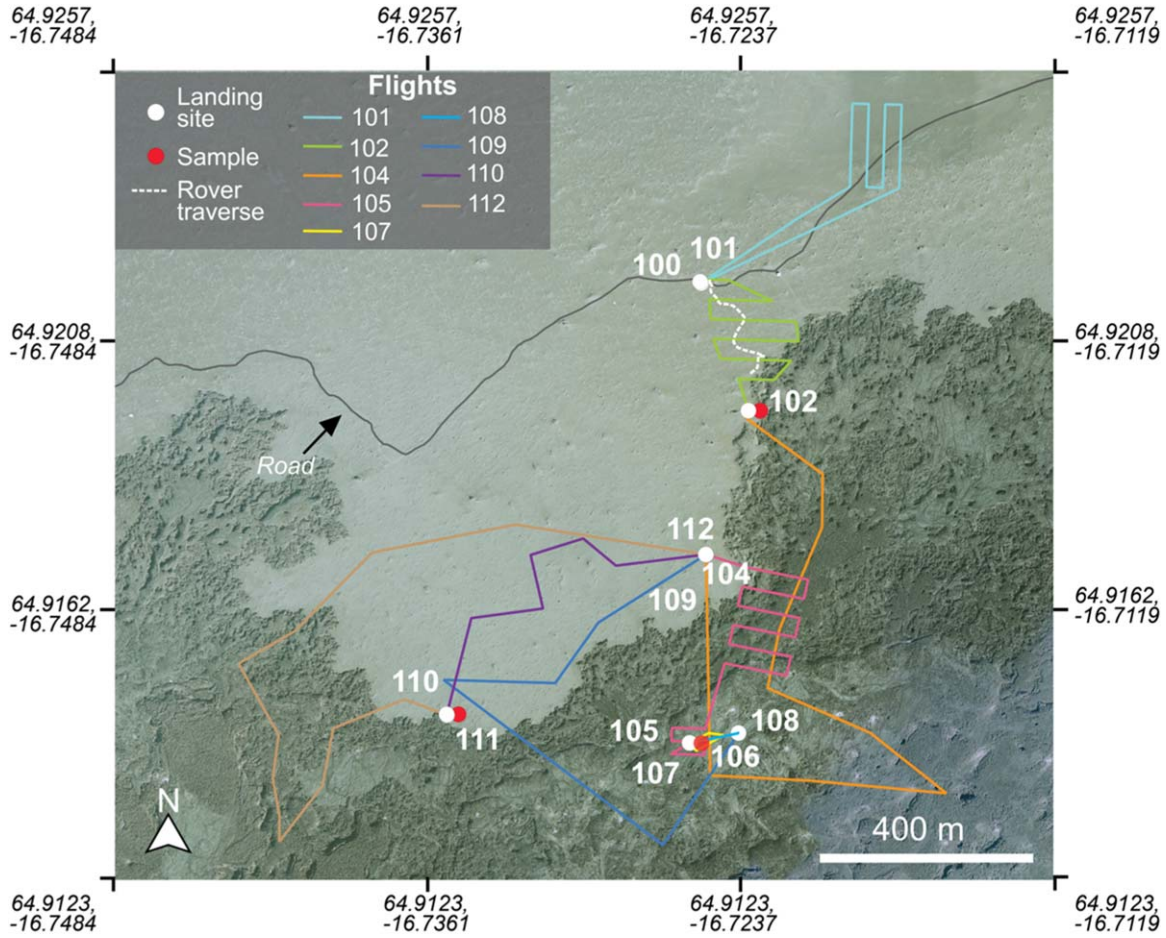

Figure 12. Map showing the 2022 helicopter mission, including landing sites (white dots), sample localities (red dots), and flight paths (colored lines). Also shown for comparison is the 2022 rover traverse (white dashed line). The base map is sourced from Loftmyndir Einkahlutafélag. (50 cm pixel^{-1}).

Table 6
Resource Allotment (Percentage) Relative to Typical Daily Constraints Imposed on the Rover and Helicopter Missions

Sol	Rover Duration %	Data Volume %	Energy %	Helicopter Duration %	Data Volume %	Energy %
101	50.28	97.07	56.00	1.16	90.48	100.06
102	32.36	99.36	31.00	1.19	98.93	99.22
103	95.28	99.57	85.25	0.00	3.35	99.33
104	54.44	24.50	88.75	1.02	97.38	93.15
105	99.72	53.57	91.75	1.37	34.50	99.29
106	63.89	18.75	92.00	0.00	3.35	99.33
107	99.99	80.03	95.81	0.05	94.60	37.51
108	47.64	99.79	44.25	0.00	0.00	0.00
109	94.17	99.18	91.00	0.88	68.99	75.54
110	66.11	52.00	100.00	0.57	73.83	59.88
111	43.75	99.86	41.25	0.00	3.35	99.33
112	66.67	14.82	99.50	1.06	97.61	90.31
113	67.22	98.29	79.25	…	…	…

8. Summary of Rover Science Results and Interpretations

8.1. Overview

Over the course of the mission, the rover science operations team succeeded in conducting detailed investigations of the older lava flow, sand sheet, and younger lava flow margin at outcrop and microscales. When compared to the HiRISE-analog data examined prelanding, the rover data significantly enhanced the team's understanding of the field site. The following sections detail the main scientific findings interpreted by the rover science operations team from the 2022 mission.

8.2. Volcanology

8.2.1. Morphology

Characterization of the older and younger lava flows at Asgard and Valhalla, respectively, supports the prelanding interpretation of at least two separate eruptive events. This

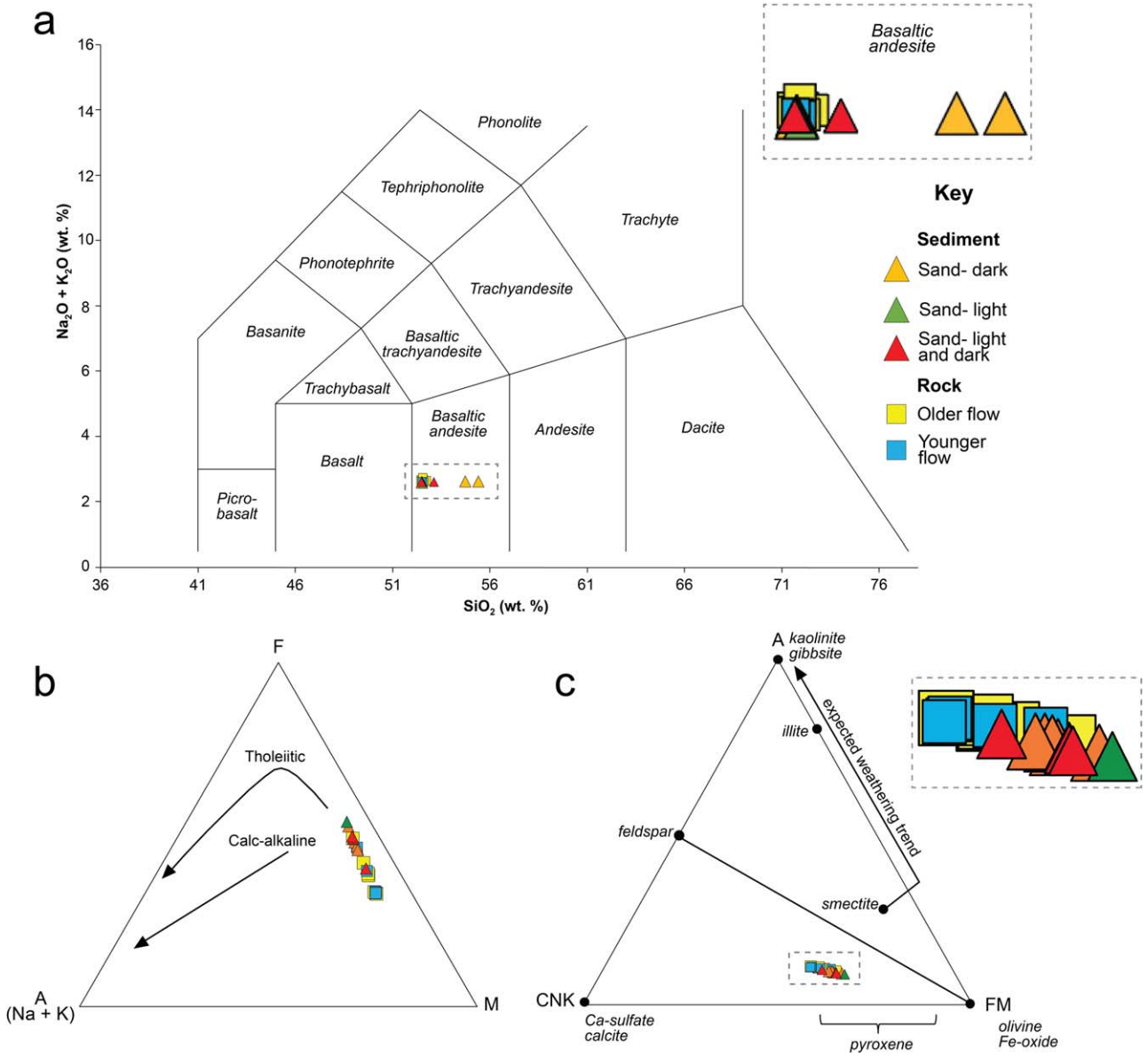

Figure 13. Geochemical trends from APXS and SuperCam LIBS data. (a) TAS diagram showing the distribution of all rock and sediment targets in the basaltic andesite field. Inset zoomed-in view shown in the larger dashed box. (b) Alkali–iron–magnesium (FAM) ternary diagram showing tholeiitic and calc–alkaline trends for reference. (c) Al_2O_3 – CaO + Na_2O + K_2O – $FeO_{(T)}$ + MgO (A–CNK–FM) ternary diagram showing the distribution of all rock and sediment targets compared to representative mineral phases and the typical mafic chemical weathering trend.

interpretation is guided by the identification of a well-defined margin for the younger flow, which is observable in the "orbiter" remote sensing data (Figure 1), the presence of the sand sheet overlying the older lava flow, and the topographic difference between both flows. These observations were confirmed in landscape-scale rover images showing sporadic exposures of the older flow covered by the sand sheet (Figures 6(a) and 9(b)) and the higher-standing, coherent, younger flow margin (Figure 9(a)).

The two flows exhibit several distinct morphologic characteristics that, in combination with topographic differences, provided support for their differentiation as separate flows. The team characterized the Asgard exposure (older flow; Figure 6(a)) as texturally rougher compared to the Valhalla exposure (younger flow; Figure 9(a)) and noted the relatively more jagged and fractured nature of the older lava flow. Valhalla and the younger flow margin appear more coherent than the older lava flow exposures (Figures 9(a) and (c)). The younger flow margin is characterized by heavily fractured, platelike features much wider than they are thick that likely represent a partially disrupted surface crust (Figure 9(c)). The team hypothesized that some of this disruption may be due to the buckling of the surface crust over the still-molten flow interior. The team interpreted these broad-scale morphological differences between the older and younger lava flows to result, in part, from the fact that Asgard represents the interior of the older lava flow surface, whereas Valhalla represents the margin of the younger lava flow. Based on the above characteristics, the sol 108 target Hel (Figure 9(b)) was determined to be part of the exposed older lava flow, enabling the team to place additional constraints on the relative location of the younger flow margin. The fragmented nature and morphological characteristics of the older flow led to identification of spiny and rubbly lava facies, whose formation involves varying

degrees of ductile to brittle deformation (see Voigt et al. 2021a, 2021b for a description of lava types and their differentiating characteristics). Although the team was unable to image the plan view surface of the younger flow margin to characterize and map out specific facies, it was reasoned based on the combined orbiter and rover data that the coherent nature of the flow margin with localized areas of apparent disruption could be consistent with the Voigt et al. (2021a) classification of spiny or undifferentiated rubbly spiny.

From contact science and close-approach images, additional characteristics were identified that further distinguished the flows. Millimeter- to centimeter-scale vesicles are pervasive in both flows (Figures 6(e) and 9(d)) but appear more variable in size and shape within the older flow. Millimeter-scale, light-toned feldspar phenocrysts and green olivine phenocrysts were commonly observed throughout the younger flow (yellow arrow in Figure 9(d)) but only sparsely identified in the older flow. Millimeter-scale veins were identified in the older lava flow at Asgard (Figure 8(a)) but not in the younger lava flow, suggesting that the associated vein-forming fluid-flow event may have predated the emplacement of the younger flow. Despite some similarities in identified morphologic features, the team identified characteristics up close that increased the confidence in the interpretation of two different flows.

8.2.2. Composition

Geochemical and mineralogical data from LIBS, simulated APXS, and VisIR showed that the elemental composition and mineralogy of the two flows were indistinguishable within instrument error. Figure 13(a) includes a total alkali–silica (TAS) plot (wt%) including all LIBS and APXS geochemical targets from the rover mission, with weighted averages calculated for all LIBS rasters (Table A2). All rock targets across both flows plot in the basaltic andesite field and primarily overlap around the same range (52.5–52.7 wt% SiO_2, 2.6–2.7 wt% $Na_2O + K_2O$). Figure 13(b) shows rock targets plotted in an A–F–M diagram (wt% $Na_2O + K_2O - FeO_{(T)} -$ MgO). Data points of both flows are distributed along a linear trend and do not plot along either the calc–alkaline trend or the tholeiitic trend, though the trend could be due to the calculated uncertainties for wt% $FeO_{(T)}$ (Table A2). Comparing the plots in Figures 13(a) and (b) further indicates that the rock targets do not follow a tholeiitic or calc–alkaline trend, and that some other factor or geochemical signature(s) may explain the composition of rocks within both flows.

Given the inconsistencies with typical mafic igneous trends, chemical weathering was evaluated as a potential driver of the geochemical signatures of both lava flows. Figure 13(c) includes the A–CNK–FM ($Al_2O3 - CaO + Na_2O + K_2O - FeO_{(T)} +$ MgO) ternary diagram, a common tool used to evaluate geochemical processes recorded in mafic rocks and sediments (e.g., weathering, diagenesis; Babechuk et al. 2014). Older and younger flow targets plot below the olivine–feldspar join, indicating that rocks from both flows are unweathered and represent primary basalt compositions. The broad geochemical overlap between the older and younger lava flows indicates that the veins identified in the older lava flow (Section 8.2.1) do not significantly influence the bulk geochemical composition. Both flows are overall geochemically similar. These similarities are further emphasized from the SuperCam VisIR spectra (Figures 10(c) and (d)) that show similar signatures of mafic olivine and pyroxene, feldspar, and little to no hydration.

8.3. Eolian Science

8.3.1. Morphology

Rover assessments of the sand sheet revealed the presence of eolian bedforms on multiple scales (Figures 8(a), (b), and 9(a)). Bedforms ranged from centimeter-scale ripples (target "Vali") to decimeter-scale sand shadows and sinuous-crested ripples (sol 107 NavCam PDI). The orientation of sinuous-crested ripples observed throughout the rover's exploration area indicates that the wind was blowing toward the north-northeast, consistent with resolvable bedforms observed in orbiter data. The majority of eolian bedforms are characterized by light-toned, coarser-grained sand mantling a dark-toned, finer-grained sediment substrate (Figure 8(b)). The light-toned sand appears to be predominantly composed of coarse sand-sized lithic grains that are subrounded to well-rounded (Figure 8(d)). The dark-toned sediment has an average grain size of fine sand. MAHLI imaging of the dark-toned sediment revealed that its dark tone was partially due to meteoric water, but drier regions also exhibit a tonal difference.

8.3.2. Composition

Sediment composition is generally similar to the older and younger lava flows (Figures 10 and 12). The TAS plot shows that both light- and dark-toned sediment populations plot within the basaltic andesite field (Figure 13(a)). Several dark-toned sediment data points plot at relatively higher wt% SiO_2 (wt% 54.7 and 55.4), possibly consistent with the hydrated silica absorption band observed in the VisIR data (Figure 10(a)). Compositional similarities between sediment and lava flows are indicated by the overlapping distribution of data in A–CNK–FM ternary space (Figure 13(c)). Although sediment targets plot at a slightly more proximal region to the FM apex, the difference is minor enough to indicate compositional similarities between the sediment and rock targets. Furthermore, data points do not plot along a typical mafic chemical weathering pathway, indicating that sediment was physically weathered from the original source rock(s). The generally similar geochemistry between the sediment and the lava flows indicates that the Holuhraun region is geochemically homogeneous and led the rover science operations team to hypothesize that sediment within the sand sheet was sourced from a geochemically similar deposit.

8.4. Habitability

To assess whether the rover's exploration area may have hosted signs of past life, the science operations team focused efforts on astrobiologically significant targets (Hadland et al. 2024). The most compelling target observed during the mission was the dark-toned, fine-grained sediment of the sand sheet. These targets were the only types to show deep and obvious hydration bands (Figure 10(a)). Although the 1.4 and 1.9 μm bands could have been due only to meteoric water, the presence of a 2.2 μm band indicates hydrated silica, which has a relatively high potential to preserve biosignatures (Cady & Farmer 1996; Farmer & Des Marais 1999). This biosignature potential also led to the decision to sample the dark-toned sand.

Several other rare astrobiological targets of interest were also identified. The team observed several millimeter-thick light-toned mineralized veins within the older flow (Figure 7(a)). Veins have been noted for their habitability and biosignature

potential on Earth and Mars (Nachon et al. 2014), although the small size and rarity of these veins prevented a definitive determination of their composition or mineralogy. Red regions identified in the rock (e.g., Figure 6(b)) could be due to oxidation, which could have been catalyzed by microbes (Hays et al. 2017). Overall, the region encountered by the rover was considered to have low habitability potential.

The team noted distinctive light-toned features visible along the margin of the younger lava flow surface in HiRISE-analog images (Figure A1). These features were interpreted to reflect fluid or gas flow along fractures and subsequent alteration of or deposition on the basalt. Such deposits were noted for their possible astrobiological significance but were inaccessible by the rover and therefore not analyzed further.

9. Summary of Helicopter Science Results and Interpretations

The helicopter science operations team used mission data to make several more detailed interpretations compared to their premission remote sensing data analysis. First, the smoother sand morphology observed during sol 101 lacked the rough outcrops of dark rock found elsewhere within the sand sheet and instead contained numerous white boulders averaging about 30 cm in diameter. This area was interpreted to not be underlain by the older lava flow and instead be a thicker sand deposit with the boulders possibly deposited by high-energy glacial outburst floods. Near the younger lava flow, the orientation of ripples in the sand plus the apparent relative thickness of sand ramp deposits on the flow margin and around other outcrops were interpreted to suggest a northeasterly direction of wind and sediment transport. Darker, finer-grained sand beneath the coarser light gray sand on the surface contained evidence of hydration, as identified by the VisIR spectrometer.

The spatial distribution and topographic relationship of surface morphologies on the younger lava flow suggested to the team that the lava in the mission area was emplaced slowly by a process of inflation and breakout. This emplacement style generates a transitional spiny morphology (Rowland & Walker 1987) that is too viscous to form a pāhoehoe texture but also too slow-moving for the crust to form an ʼāʼā texture. White discoloration was observed along cracks in the flow crust on the surface of the younger flow. Although this discoloration was not chemically distinct from the flow (which the helicopter science operations team noted may be due to instrument error; Carr et al. 2024), it was interpreted to be mineral precipitation from degassing of the flow interior during and after emplacement. Outcrops of the older lava flow were too isolated to draw any strong conclusions about emplacement mechanisms, but the team did note that the morphologies exposed were different compared to the younger lava flow, suggesting the older flow had different emplacement mechanisms and/or composition compared to the younger lava flow.

Regarding habitability, the helicopter science operations team interpreted light-toned features on the younger lava flow surface as evidence of hydrothermal precipitation and concluded that such features may be astrobiologically significant. The sparse occurrence of these features and the lack of other evidence for biological activity led the helicopter science operations team to conclude that the region encountered by the helicopter had low habitability potential.

10. Discussion

10.1. Rover Mission

The RAVEN rover mission was successful in collecting a data set and sample suite that adequately addressed the mission's eolian, volcanology, and habitability science objectives (Figure 2) and corroborated the premission hypothesis that differentiated two separate lava flows through identification of morphologic, topographic, and minor mineralogical differences. The main operational limitation experienced by the rover science operations team during the mission simulation was related to the rover's mobility, particularly the power and duration needed to drive the rover. With a maximum daily traverse distance of ∼100 m, as well as other sampling and science objectives to achieve, the rover made it only to the margin of the younger flow. Traversing up and onto the flow was also prohibited both by the topography and slope of the margin and by the limited duration of the field simulation. These limitations prevented the team from acquiring additional ground-based observations of the different lava flow facies that are known to comprise the younger flow (Voigt et al. 2021a). Thus, the team's knowledge and understanding of the younger flow were limited to the morphologies that were observed from orbiter data and the front of the Valhalla exposure at the flow margin. Nonetheless, the acquired images of the younger flow thoroughly captured and characterized the observable variation within the rover's exploration area, which, along with the acquired sample, achieved the science objectives for this unit. Additionally, the accessibility of the older lava flow and sand sheet enabled the team to conduct detailed investigations of these units that resulted in acquisition of data that could successfully address the science and sampling objectives.

Like past and present Mars rovers, the main strength of the RAVEN rover payload was its capability to interrogate a workspace down to the micron scale. While the resolution of the HiRISE-analog images could permit interpretations of the Holuhraun region as a series of basaltic lava flows, rover instrument capabilities enable reconciliation of orbital-scale geomorphic observations with micron-scale features and composition. For example, premission assessments concluded that there were two lava flows present in the mission area, but MAHLI images showed that a key difference between the two flows was the common presence of visible phenocrysts in the younger lava flow and the lack of abundant phenocrysts in the older lava flow. Millimeter-scale assessments also provided the team with direct guidance for sample selection. For example, the sample "Mjolnir" (Figure 7(a)) was chosen to target millimeter-scale mineralized veins that were identified in MAHLI images of the "Ragnarok" sampling location.

Several rover capabilities that could not be accurately simulated in the RAVEN mission should be recognized when discussing the high-resolution analytical capabilities of a rover payload. One of the critical capabilities of conducting remote geological analysis with a rover payload is the ability to abrade a "fresh" rock surface of which high-resolution images enable resolution of micron-scale features (Indyk et al. 2018; Moeller et al. 2021). On the Mars 2020 Perseverance rover, abrasion of rock surfaces produces polished surfaces from which grain-scale features can be better resolved, enabling the team to interpret important information about the rock fabric (e.g., lithology, grain or phenocryst size, matrix composition, grain coatings, cements, alteration). During the RAVEN rover

mission, the simulated abrasions on both lava flow sample sites could not polish the rock surface to the expected degree of a typical abrader but resulted in scratched surfaces that largely obscured any features or fabrics of interest. While the team was subsequently unable to conduct detailed image analyses of abrasion patches, it can be assumed that such information would have been readily available for analysis using a realistic rover abrasion tool. This study therefore emphasizes the rover abrasion tool as an important asset used for micron-scale geological investigations at each sampling locality. Another high-resolution technique utilized with the Curiosity and Perseverance rovers involves analyses of the fine-grained drill tailings generated from drilling into rock (e.g., Jacob et al. 2020). This capability enables remote sensing instruments to acquire compositional data on the drilled sample and in doing so provides a valuable geochemical data point to compare to mineralogical measurements (on board Curiosity) or future lab analysis (Mars Sample Return). Although these techniques were not fully simulated in this exercise, this study recognizes the analysis of abrasion patches and drill tailings as essential strengths of a rover payload. Another important capability of rover missions is the lab-quality payloads that are unique to the rover, which the RAVEN rover mission could not adequately simulate in their entirety, e.g., the Sample Analysis at Mars (Mahaffy et al. 2012) and the Chemistry and Mineralogy (Blake et al. 2012) instruments on the Curiosity rover and the Planetary Instrument for X-Ray Lithochemistry (Allwood et al. 2020) and SHERLOC (Bhartia et al. 2021) instruments on the Perseverance rover.

Changes to the science operations team's strategic plan were made during the simulation in response to tactical science discoveries. The main change to the strategic plan responded to the discovery of the dark-toned sand underlying the light-toned coarse-grained sand (Figure 8(b)). Upon identifying hydrated silica within the dark-toned sediment (Figure 10(a)), the team subsequently prioritized the collection of an additional sample of the dark-toned sediment (Figure 7(d)) at the expense of additional time spent at the younger flow-front margin, which compositionally appeared very similar to the older lava flow already examined. This decision resulted in changes to the sol path and provided justification for the team to acquire a second eolian sample.

Minor changes were made to the plan to accommodate trade-offs between engineering and science priorities. For example, the sol 106–107 plan required several changes to science observations to prioritize a lengthier drive to the Valhalla exposure. Because of the resources needed to execute the planned traverse, SuperCam and MastCam activities on nearby eolian features were descoped from the plan. These changes did not significantly impact the team's scientific interpretations of the site, so the trade was deemed worthwhile to ensure that the rover would arrive at the younger flow margin within the time limits of the mission simulation.

10.2. Comparison between Rover and Helicopter Mission Architectures

One of the primary motivations for the RAVEN project to run separate rover and helicopter missions was to create baselines against which the capabilities of a combined rover–helicopter mission could be compared. To this end, it is useful to critically examine the strengths and limitations of the rover and helicopter mission architectures individually, with respect to overall RAVEN science mission goals.

10.2.1. Mission Implementation and Outcomes

While the rover and helicopter missions were both successfully completed within the allotted 14 sol timeline, the two missions chose to allocate their time differently (Figure 11(a)). Compared to the helicopter mission, the rover spent a more even distribution of sols across each of the three phases: older lava flow (six sols), sand sheet (four sols), and younger lava flow (three sols). By contrast, the helicopter mission spent very little time studying the older lava flow and conducted most of its mission at the younger lava flow (eight sols). This decision was, in part, due to landing site hazards on the older lava flow. The helicopter was able to land near an exposure of the older flow, but collision hazards prevented a closer approach and landed science observations (Carr et al. 2024). Smooth surfaces on the younger flow were sufficient for the helicopter to land and conduct contact science, enabling a more extensive campaign. As a result, the helicopter science operations team acquired both of their mission's volcanic samples on the younger lava flow, whereas the rover science operations team was able to acquire a sample of both the older and younger lava flows.

The total distance flown by the helicopter (10 km) was significantly greater than the total distance traversed by the rover (245 m). The helicopter therefore obtained greater total spatial coverage of the region (Figure 12), having conducted a mapping survey flight across the entire length of the rover mission's traverse on a single sol. One result of the greater flight distance per sol was that the helicopter was able to capture and map variable morphologies and flow facies within the younger lava flow, albeit at altitudes of tens of meters. In contrast, the rover visited only one site along the margin of the younger flow and was unable to acquire any data documenting the areal distribution of flow morphology beyond what could be observed in HiRISE-analog data. However, the rover was able to conduct investigations at a significantly greater level of detail than the helicopter due to its targeting capabilities. For example, the rover acquired 17 targeted MAHLI images at different standoff distances on six unique targets, six of which were of abrasion patches and four of which were of the drill boreholes. In addition, RMI images were acquired on 22 unique targets, including abrasion patches. Such images could resolve micron- to millimeter-scale features such as grains, phenocrysts, microfractures, and small-scale igneous textures (e.g., Figures 6(e) and 9(d)). In contrast, the helicopter acquired seven MAHLI images of the ground while landed (Carr et al. 2024) but was constrained to a fixed pointing at a lower resolution with limited input from the helicopter science operations team.

Both systems varied in their use of duration, power, and data volume. Figure 11(b) shows the percentage of resources relative to the maximum allotted values for each mission. Data volume and energy were commonly limiting resources for both the rover and the helicopter missions. For the rover, data volume was the limiting resource on sols with predrive targeted remote science blocks (Table 5) due to the extensive data usage of the MastCam and NavCam mosaics (4500–67,500 kB), MAHLI images (6000–24,000 kB), and SuperCam activities (2000–10,000 kB). For the helicopter, data volume was the main limiting resource, and the DEMs and orthomosaics

produced from images captured during survey flights comprised the highest data volume usage (Carr et al. 2024). Due to this finding, the helicopter science operations team opted to conduct survey flights only over areas of high science priority. Data volume-limited sols for the helicopter mission (sols 104, 107, 110, and 112) involved extensive in-flight images or downlinked survey products (∼17,000 kB). Energy-limited sols on the rover mission (sols 103, 104, 106, 110, and 112) involved abrasion and sampling activities (100–255 Wh), whereas energy-limiting sols on the helicopter mission (101, 102, 103, 105, 106, and 111) involved either sampling activities (46.8 Wh) or mapping surveys (126.7–198.5 Wh). Given the relatively short flight times, duration was not a limiting resource on the helicopter mission (Carr et al. 2024), highlighting the large distance:time value of this mission approach. However, the helicopter's data volume and power limitations meant that much of this terrain was only cursorily characterized by the helicopter. Only two sols of the rover mission were duration-limited, and both involved lengthy drives (86 m on sol 105 and 70 m on sol 107; Table 5). Overall, the main resource-limiting activities for both missions were sampling-related activities. The main differences in resource usage between both missions derived from the data volume- and energy-intensive helicopter survey flights and individual airborne images and the duration-intensive rover drives.

A main difference between the missions' operations approach pertained to sampling and depot strategy. While the rover had the capability to collect samples additively, constructing a sample depot at the very end of the mission simulation, the helicopter had to return to the same depot site because it did not have multiple sample storage capabilities. This constraint, which the RAVEN team imposed on itself so that both missions would create comparable sample depots, created a leash for the helicopter relative to the depot site, limiting the distance and area that the helicopter could fly and sample. A strategy of dropping samples as they are collected would have removed this constraint for the helicopter science operations team but would not have created a sample depot directly comparable with the rover sample depot.

Both missions used the same general operations process whereby assessment of downlinked data from previous sols was used to inform tactical decisions. Whereas the rover science operations team used NavCam mosaics to pick specific targets in the workspace for contact and remote observations, the helicopter science operations team used acquired images to decide on scientific targets and identify accessible landing sites. Although both systems operated in response to downlinked data, the lack of targetability beyond the point directly below the helicopter meant that much of the helicopter operations were decided strategically. Additionally, one key difference between the missions was the type and scale of opportunistic science observations added to the plans. Given the helicopter's relatively low-cost ability to cover large distances very quickly, the helicopter science operations team decided to divert to a potential outburst flood deposit to the northeast of the starting site (Carr et al. 2024). A diversion such as this would have been incredibly costly for the rover mission and would likely have prevented the rover from achieving its goal of reaching the younger flow margin within the duration of the mission simulation. However, this diversion had a minimal impact on the helicopter mission's main exploration and sampling objectives.

The main opportunistic decision made by the rover science operations team involved investigation and sampling of the dark-toned sediment, which was not previously identified from prelanding orbiter data. The rover science operations team also observed light-toned vuggy features in the Asgard workspace and chose to investigate these features (Section 7.2). These are features at a scale ideally suited for the payload and perspective of a rover mission and thus were followed up on by the rover science operations team via targeted imaging and compositional observations and contact science. In contrast, the helicopter was limited in its ability to detect features at this scale and lacked a payload that would enable further detailed, targeted investigation.

10.2.2. Comparison of Science Interpretations

At a high level, both the rover and helicopter missions came to the same scientific conclusions about the geology of the exploration area and the origin and age relationships of the three main geologic units (older lava flow, sand sheet, and younger lava flow). However, the scope of these interpretations differed between missions largely due to differences in payload implementation and individual science expertise of the respective mission science operations teams.

Both teams recognized the existence of an older flow and a younger flow and concluded that different meter-scale morphologies within the flows were linked to flow emplacement processes. While the helicopter science operations team focused on documenting and characterizing flow morphology variations on the surface of the younger flow over a wide, kilometer-scale area (Figure 13; Carr et al. 2024), the rover science operations team focused on the observation and documentation of features in cross-sectional views of the flows at Asgard and Valhalla. The larger area observed by the helicopter mission allowed the helicopter science operations team to use the distribution of flow morphology and topographic relationships between different parts of the flow to approximate an eruption history and emplacement rate for the younger lava flow (Carr et al. 2024). This level of detailed interpretation was not possible with the data collected by the rover team. While the rover science operations team was able to conduct a detailed investigation of grain-scale textures and fabrics within the older lava flow, the helicopter science operations team's investigation of the older flow was limited to aerial views at a distance of tens of meters, since a safe landing site on this terrain could not be found. The rover science operations team acquired geochemistry and mineralogy data for both the older flow and the younger flow (Figures 10(c), (d), and 13(a)), while the helicopter science operations team acquired compositional data only for the younger flow (Carr et al. 2024).

Within sand sheet deposits, both teams were able to identify at least two classes of eolian bedforms based on size. Both teams interpreted a north-northeast wind direction based on bedform orientation (Carr et al. 2024), although the rover science operations team was able to clearly identify stoss and lee sides of individual ripples given the rover's imaging perspective. The lower resolution of the helicopter data (because of its greater distance from the features) limited the identification of stoss and lee faces of individual ripples. The enhanced imaging capabilities of the rover enabled high-fidelity observation and measurement of grain sizes on multiple targets for the dark- and light-toned sediment. While the

helicopter's MAHLI image of the sediment sample site could resolve grains, the lower apparent resolution and limited targeting capabilities inhibited the team's ability to characterize the sand sheet more thoroughly. Compositional VisIR data on dark-toned sand from both systems showed hydrated signatures (Figure 10(a); Carr et al. 2024).

The habitability assessments from both missions differed due to the scale and accessibility of astrobiologically significant features. One common finding between systems regarding habitability was the documentation of hydrated silica within the dark-toned sand (Figure 10(a); Carr et al. 2024). The rover science operations team interpreted occurrences of millimeter-scale light-toned mineralized veins within the older lava flow (Figure 7(a)) as astrobiologically compelling targets, whereas the helicopter science operations team was unable to find or resolve these small-scale veins in their image data set. The helicopter science operations team observed and measured with LIBS and VisIR white-colored deposits or stains associated with larger fractures observed on the younger lava flow surface (Carr et al. 2024), which the rover did not visit and could not access within the constraints of the mission simulation. Despite the inaccessibility of the younger lava flow fractures for the rover, some of these light-toned alteration zones are visible in the orbiter data and were noted by the rover science operations team prelanding.

10.2.3. Mission Comparisons and Implications for Future Studies

Comparisons of mission results and scientific interpretations confirm that rover and helicopter payloads can observe and interpret similar geologic features in an exploration area, especially with the addition of HiRISE-analog data, but the payloads will generate data sets and interpretations that vary in scope and scale. Despite the largely similar terrain covered by both systems, each mission differed in terms of traversability. These differences are partially due to the resource-intensive nature of rover drives compared to helicopter flights. The helicopter mission had an advantage in terms of distance covered and diversity of terrain imaged, but the rover was able to obtain more, and more detailed (higher-resolution), observations at each feature of interest with targeting input from the team. While the rover's mobility limited the distance and areas it could reach, the helicopter's landing constraints also proved limiting in some cases (e.g., unable to sample the older lava flow). The difference in each system's mobility across the same terrain facilitated data sets that differed in scale, with the rover payload better suited for detailed geologic and compositional interrogation (e.g., more targets with measurable grain sizes and shapes and recognition of microscale features such as vuglike features, phenocrysts, and mineralized veins). Although the helicopter payload could resolve millimeter-scale features, the lack of high-resolution targeting capabilities meant that the helicopter was better suited for meter-scale mapping of surface morphologies. In the seemingly homogeneous setting encountered by the rover, the helicopter views of the lava flow morphology of the younger flow offered additional insights into the emplacement history of Holuhraun and the differing characteristics of both flows.

Additionally, each payload provided different perspectives on similar features. The rover obtained mosaics showing cross-sectional perspectives of the younger lava flow margin that could be used to supplement the surface views of this region provided by the orbiter data. The helicopter provided higher-resolution images of the surface than the orbiter-analog data but offered limited ground-eye views of the terrain and geology. Given the rover science operations team's assessment of a geologically homogeneous setting at Holuhraun, the helicopter views of the lava flow morphology of the younger flow offered additional insights into the emplacement history of the lava and the differing characteristics of both flows. However, the strengths of each system as applied to the investigation of the Holuhraun region would differ in geologically different settings. For example, when assessing a succession of sedimentary rocks, the most diagnostic observations are often on the vertical faces of layering at grain-scale resolutions. This scenario would be better suited to a rover, which can acquire high-resolution cross-sectional views of targeted sedimentary structures and facies to enable better reconciliation with larger-scale stratigraphic context. In contrast, a helicopter payload would be useful for documenting more generalized stratigraphic relationships at coarser resolutions, particularly for regions that are inaccessible to a rover. In a combined rover and helicopter mission, these two systems would ideally be utilized in concert with one another in order to extract the most data at all possible scales, but this scenario depends on accessibility of each system with respect to the field area.

The assessments from the individual RAVEN missions can inform possible future combined rover and helicopter mission operations strategies. One challenge in combining the two different systems into one mission would be the complexity and logistics associated with the daily mission operations schedule. As exhibited on Mars rover missions (e.g., Vasavada 2022), assembling a tactical plan typically requires the full allotted time for that meeting, and meeting schedules are immovable based on the timing of data uplink and downlink. Planning for a second system during this tactical planning schedule would therefore not be feasible. Given that the helicopter does not respond to downlinked data at the same cadence as the rover and can often plan flights and observations more strategically based on orbiter data, helicopter planning may be better suited to occur during the campaign implementation meeting (Table 3). This would enable the planning of a dual-system mission within the restrictions of the typical daily planning schedule.

Given the different capabilities and resolutions between the rover and helicopter payloads, a combined rover–helicopter mission has the potential to increase a mission's scientific return but would be limited by its resource usage. Helicopters can be utilized to scout locations for future rover traverses (Golombek et al. 2022). However, the large data volume of the image surveys would potentially require several sols worth of relay passes to fully downlink, severely limiting the number of rover activities that can be simultaneously conducted. To take advantage of rover traverse planning with helicopter data, a reduced cadence of rover and helicopter activities would have to be implemented and should only include additional science activities that are relatively low in data volume and do not require ground-in-the-loop decision-making. This could be problematic for a rover-based mission, which typically involves very restricted schedules and requires constant rover operation and resource usage. Given these constraints, a more optimal scenario could have the helicopter operate at a similar cadence as the Mars helicopter Ingenuity, where flights occurred at most several times per month rather than daily like the RAVEN helicopter mission. Additionally, the helicopter data would be

downlinked nondecisionally in order to prioritize decisional acquisition of the necessary rover data for targeted tactical planning. This scenario would treat the helicopter as more of a support payload for the rover rather than a stand-alone payload that is emphasized to the same extent as the rover. An additional option could include descoping the image survey activities meant for rover scouting to single or multiple images, which would reduce the data volume. Future studies involving a combined rover and helicopter mission architecture will have to prioritize reconciliation of desired activities with data volume limitations.

Overall, the findings in this study indicate that a combined rover and helicopter mission leveraging the strengths of each system could result in a powerful and capable mission architecture but must take into consideration system capabilities (e.g., traverse or flight distance) and connectivity and resource usage as well as geologic characteristics that may be unique to the mission site when making tactical and long-term strategic decisions.

11. Conclusions

1. This study details the planning, implementation, and results from the 2022 RAVEN rover mission in a Mars analog site in Iceland and compares the results with the 2022 RAVEN helicopter study.
2. The rover science operations team planned a successful 14 sol mission, 13 sols of which were executed in the field, that achieved mission, science, and sampling goals and was successfully executed in the field by the field implementation team.
3. The rover payload and targetability enabled more detailed investigations and interpretations of texture, morphology, and composition of all three units mapped prior to landing: (1) an older lava flow, (2) a sand sheet, and (3) a younger lava flow.
4. The helicopter capabilities enabled greater spatial coverage of the exploration area, with emphasis on the younger lava flow.
5. Based on the individual capabilities of each system, each team tactically planned opportunistic science on different features of interest: the helicopter science operations team aimed to increase terrain diversity, whereas the rover science operations team pursued more detailed follow-up observations of microscale features.
6. The main differences in resource usage between both missions involved the data volume and energy usage of helicopter survey flights and individual in-flight images and the duration of lengthy rover drives.
7. A combined rover and helicopter scientific study on Mars should consider how to optimize the different capabilities of each system, also accounting for differences in system strengths based on regional geology.
8. Future combined rover and helicopter missions will need to address the issue of data volume as the primary limiting resource. This issue could partially be solved with a reduced cadence of helicopter operations relative to the RAVEN helicopter mission and strategic planning of the helicopter activities during operations shifts.

Acknowledgments

This research was carried out in part at the Jet Propulsion Laboratory, California Institute of Technology, under a contract with the National Aeronautics and Space Administration. This study was supported by NASA PSTAR grant No. 80NSSC21K0011. This work was partially funded through a Canadian Space Agency FAST grant to Catherine Neish (21FAUWOB01). We are grateful to the entire RAVEN team for helping to develop and implement the analog science mission simulations. We acknowledge Catherine Neish (University of Western Ontario) and Gavin Tolometti (Skywatch) for their support and mentorship. We thank the Vatnajökull National Park Service (Vatnajökulsþjóðgarður) for providing permission to work in the Holuhraun region and the Icelandic Institute of Natural History (Náttúruminjasafn Íslands) for permission to collect and export samples. We thank the editor and two reviewers for their thorough feedback that greatly improved the quality of this manuscript.

Appendix

Figure A1 shows a remotely sensed image of light-toned zones of alteration on the younger lava flow. Table A1 includes all of the rover activities from the 2022 mission, and Table A2 includes the rover-acquired LIBS and APXS data.

Table A1
All Rover Activities from the 2022 Mission

Sol	Type	Description	Duration (minutes)	Data Usage (kB)	Energy Usage (Wh)	Frames	Drive Distance
101	SuperCam power ON	Power on SuperCam	10	90	4	N/A	
101	SuperCam LIBS 5 points	LIBS of sand target Heimdall	12	10,000	10	N/A	
101	SuperCam RMI image	RMI of target Heimdall	1	2000	2	N/A	
101	SuperCam LIBS 5 points	LIBS of rock target Loki	12	10,000	10	N/A	
101	SuperCam RMI image	RMI of target Loki	1	2000	2	N/A	
101	SuperCam LIBS 5 points	LIBS of rock target Thor	12	10,000	10	N/A	
101	SuperCam RMI image	RMI of target Thor	1	2000	2	N/A	
101	SuperCam power OFF	Power off SuperCam	4	10	1	N/A	
101	MastCam mosaic—Z30	7 x 1 (top row 4, bottom row 3) mosaic of ripples for wind direction and morphology	9	31,500	16	7	
101	MastCam mosaic—Z100	MCAM Doc of SuperCam target Heimdall	3	4500	4	1	
101	MastCam mosaic—Z100	MCAM Doc of SuperCam target Loki	3	4500	4	1	
101	MastCam mosaic—Z100	MCAM Doc of SuperCam target Thor	3	4500	4	1	
101	Rover traverse—directed drive	Drive to location Asgard	55	1800	72	N/A	18

Table A1
(Continued)

Sol	Type	Description	Duration (minutes)	Data Usage (kB)	Energy Usage (Wh)	Frames	Drive Distance
101	NavCam panorama	NCAM PDI pano	25	20,000	25	N/A	
101	MastCam mosaic—workspace PDI	N/A	8	27,000	14	N/A	
101	MastCam image—clast survey	N/A	3	6000	4	N/A	
101	SuperCam power ON	Power on SuperCam	10	90	4	N/A	
102	SuperCam LIBS 5 points	LIBS of target Freya	12	10,000	10	N/A	
102	SuperCam RMI image	RMI of target Freya	1	2000	2	N/A	
102	SuperCam LIBS 5 points	LIBS of target Frigg	12	10,000	10	N/A	
102	SuperCam RMI image	RMI of target Frigg	1	2000	2	N/A	
102	SuperCam power OFF	Power off SuperCam	4	10	1	N/A	
102	MastCam mosaic—Z100	Z100 Doc of SuperCam targets Frigg and Freya	3	4500	4	1	
102	MastCam mosaic—Z30	5 x 2 mosaic of target Asgard	12	45,000	22	10	
102	MastCam mosaic—Z100	2 x 2 mosaic of target Odin	6	18,000	10	4	
102	Rover traverse—directed drive	Bump drive to location Ragnarok	22.5	500	20	N/A	5
102	NavCam panorama	NCAM PDI pano	25	20,000	25	N/A	
102	MastCam mosaic—workspace PDI	N/A	8	27,000	14	N/A	
102	SuperCam power ON	Power on SuperCam	10	90	4	N/A	
103	SuperCam VisIR 5 points	VisIR of target Baldur	12	10,000	10	N/A	
103	SuperCam LIBS 5 points	LIBS of target Baldur	12	10,000	10	N/A	
103	SuperCam RMI image	RMI of target Baldur	1	2000	2	N/A	
103	SuperCam VisIR 5 points	VisIR of target Vili	12	10,000	10	N/A	
103	SuperCam LIBS 5 points	LIBS of target Vili	12	10,000	10	N/A	
103	SuperCam RMI image	RMI of target Vili	1	2000	2	N/A	
103	SuperCam RMI image	RMI of target Ve	1	2000	2	N/A	
103	SuperCam power OFF	Power off SuperCam	4	10	1	N/A	
103	MastCam mosaic—Z100	5 x 3 Mosaic Ragnarok including SuperCam targets Vili and Ve	17	67,500	32	15	
103	MastCam mosaic—Z100	1 x 1 Doc image of SuperCam target Baldur	3	4500	4	1	
103	Arm—unstow	N/A	20	500	45	N/A	
103	Arm—place on target	Target Mjolnir	10	500	20	N/A	
103	Rock abrasion	Target Mjolnir	90	500	100	N/A	
103	Arm—move	N/A	10	500	30	N/A	
103	NavCam	Navcam L Ragnarok workspace	5	50	1	N/A	
103	NavCam	Navcam R Ragnarok workspace	5	50	1	N/A	
103	Arm—place on target	Place on target Mjolnir	10	500	20	N/A	
103	MAHLI standard suite (25, 5, 2 cm standoff)	Target Mjolnir	8	18,000	8	N/A	
103	Arm—instrument swap	N/A	10	200	15	N/A	
103	APXS—daytime medium 90 minutes	Integration on target Mjolnir	90	500	14	N/A	
103	Arm—move	N/A	10	500	30	N/A	
104	SuperCam power ON	Power on SuperCam	10	90	4	N/A	
104	SuperCam VisIR 5 points	VisIR of Mjolnir abrasion	12	10,000	10	N/A	
104	SuperCam LIBS 5 points	LIBS of Mjolnir abrasion	12	10,000	10	N/A	
104	SuperCam RMI image	RMI image of Mjolnir abrasion	1	2000	2	N/A	
104	SuperCam power OFF	Power off SuperCam	4	10	1	N/A	
104	MastCam mosaic—Z100	1 x 1 Z100 Doc image of SuperCam target Mjolnir abrasion	3	4500	4	1	
104	Arm—place on target	N/A	10	500	20	N/A	
104	Sample acquisition	Sample target Mjolnir	120	500	255	N/A	
104	Arm—instrument swap	N/A	10	200	15	N/A	
104	MAHLI single image	5 cm standoff of Mjolnir borehole	4	6000	4	N/A	
104	Rover traverse—autonav drive	40 m drive	160	8000	160		40
105	MastCam image—clast survey	Mid-drive clast survey	3	6000	4	N/A	
105	Rover traverse—autonav drive	~40 m drive (or to end of day) that fits with PDI, turn for comm to RNAV Az +90	160	8000	160		40

Table A1
(Continued)

Sol	Type	Description	Duration (minutes)	Data Usage (kB)	Energy Usage (Wh)	Frames	Drive Distance
105	NavCam panorama	N/A	25	20,000	25	N/A	
105	MastCam mosaic—workspace PDI	N/A	8	27,000	14	N/A	
105	MastCam image—clast survey	N/A	3	6000	4	N/A	
105	Arm—unstow	N/A	20	500	45	N/A	
106	Arm—place on target	Target Njord	10	500	20	N/A	
106	MAHLI mosaic	4 × 1 5 cm standoff of target Njord	10	24,000	10	4	
106	Arm—instrument swap	N/A	10	200	15	N/A	
106	APXS—daytime short 45 minutes	APXS observation of target Njord	45	300	7	N/A	
106	Arm—instrument swap	N/A	10	200	15	N/A	
106	Sample acquisition	Target Njord	120	500	255	N/A	
106	NavCam	NavCam L of Njord sample site	5	50	1	N/A	
106	SuperCam power ON	Power on SuperCam	10	90	4	N/A	
107	SuperCam VisIR 3 points	3 × 1 VisIR of target Niflheim	7	6000	6	N/A	
107	SuperCam LIBS 3 points	3 x 1 LIBS of target Niflheim	7	6000	6	N/A	
107	SuperCam RMI image	RMI of target Niflheim	1	2000	2	N/A	
107	SuperCam VisIR 5 points	5 x 1 VisIR of target Muspelheim	12	10,000	10	N/A	
107	SuperCam LIBS 5 points	5 x 1 LIBS of target Muspelheim	12	10,000	10	N/A	
107	SuperCam RMI image	RMI of target Muspelheim	1	2000	2	N/A	
107	SuperCam power OFF	Power off SuperCam	4	10	1	N/A	
107	MastCam mosaic—Z100	1 x 1 Doc image of SuperCam target Muspelheim	3	4500	4	1	
107	MastCam mosaic—Z100	1 x 1 Doc image of SuperCam target Niflheim	3	4500	4	1	
107	Rover traverse—autonav drive	Drive to location near Valhalla	263.95	13,940	278.8		69.7
107	NavCam panorama	NCAM PDI pano	25	20,000	25	N/A	
107	MastCam mosaic—workspace PDI	N/A	8	27,000	14	N/A	
107	MastCam image—clast survey	N/A	3	6000	4	N/A	
107	SuperCam power ON	Power on SuperCam	10	90	4	N/A	
108	SuperCam VisIR 5 points	5 x 1 VisIR of target Hel	12	10,000	10	N/A	
108	SuperCam LIBS 5 points	5 x 1 LIBS of target Hel	12	10,000	10	N/A	
108	SuperCam RMI image	RMI of target Hel	1	2000	2	N/A	
108	SuperCam power OFF	Power off SuperCam	4	10	1	N/A	
108	MastCam mosaic—Z100	1 x 1 Z100 Doc image of SuperCam target Hel	3	4500	4	1	
108	MastCam mosaic—Z100	9 x 1 mosaic toward Valhalla (top)	11	40,500	20	9	
108	MastCam mosaic—Z100	2 x 1 mosaic toward Valhalla (bottom)	4	9000	6	2	
108	Rover traverse—directed drive	Bump to Yggdrasil sample location	47.5	1500	60		15
108	NavCam panorama	NCAM PDI pano	25	20,000	25	N/A	
108	MastCam mosaic—workspace PDI	N/A	8	27,000	14	N/A	
108	AEGIS analysis	Search for dark float rocks	5	1000	2		
108	SuperCam power ON	Power on SuperCam	10	90	4	N/A	
108	SuperCam LIBS 3 points	LIBS of AEGIS_108a	7	6000	6	N/A	
108	SuperCam VisIR 3 points	VisIR of AEGIS_108a	7	6000	6	N/A	
108	SuperCam RMI image	RMI of AEGIS_108a	1	2000	2	N/A	
108	SuperCam power OFF	Power off SuperCam	4	10	1	N/A	
108	SuperCam power ON	Power on SuperCam	10	90	4	N/A	
109	SuperCam VisIR 3 points	VisIR of workspace target Fenrir	7	6000	6	N/A	
109	SuperCam LIBS 3 points	LIBS of workspace target Fenrir	7	6000	6	N/A	
109	SuperCam RMI image	RMI of workspace target Fenrir	1	2000	2	N/A	
109	SuperCam VisIR 5 points	VisIR of target Aegir	12	10,000	10	N/A	
109	SuperCam LIBS 5 points	LIBS of target Aegir	12	10,000	10	N/A	
109	SuperCam RMI image	RMI of target Aegir	1	2000	2	N/A	
109	SuperCam power OFF	Power off SuperCam	4	10	1	N/A	
109	MastCam mosaic—Z100	5 x 3 mosaic of workspace Yggdrasil including target Fenrir	17	67,500	32	15	
109	MastCam mosaic—Z100	3 x 1 mosaic of SuperCam target Aegir	5	13,500	8	3	

Table A1
(Continued)

Sol	Type	Description	Duration (minutes)	Data Usage (kB)	Energy Usage (Wh)	Frames	Drive Distance
109	Arm—unstow	N/A	20	500	45	N/A	
109	Arm—place on target	Target Fenrir	10	500	20	N/A	
109	Rock abrasion	Target Fenrir	90	500	100	N/A	
109	Arm—move	N/A	10	500	30	N/A	
109	NavCam	NavCam L of Yggdrasil workspace	5	50	1	15	
109	Arm—place on target	Place on target Fenrir	10	500	20	N/A	
109	MAHLI standard suite (25, 5, 2 cm standoff)	MAHLI target Fenrir	8	18,000	8	N/A	
109	Arm—instrument swap	N/A	10	200	15	N/A	
109	APXS—daytime medium 90 minutes	APXS integration on target Fenrir	90	500	14	N/A	
109	Arm—move	N/A	10	500	30	N/A	
109	SuperCam power ON	Power on SuperCam	10	90	4	N/A	
110	SuperCam VisIR 5 points	VisIR of Fenrir abrasion	12	10,000	10	N/A	
110	SuperCam LIBS 5 points	LIBS of Fenrir abrasion	12	10,000	10	N/A	
110	SuperCam RMI image	RMI of Fenrir abrasion	1	2000	2	N/A	
110	SuperCam VisIR 5 points	VisIR of target Jord	12	10,000	10	N/A	
110	SuperCam LIBS 5 points	LIBS of target Jord	12	10,000	10	N/A	
110	SuperCam RMI image	RMI of target Jord	1	2000	2	N/A	
110	SuperCam power OFF	Power off SuperCam	4	10	1	N/A	
110	MastCam mosaic—Z100	1 x 1 Z100 Doc SuperCam target Fenrir abrasion	3	4500	4	1	
110	MastCam mosaic—Z100	1 x 1 Z100 Doc SuperCam target Jord	3	4500	4	1	
110	Arm—place on target	N/A	10	500	20	N/A	
110	Sample acquisition	Sample target Fenrir	120	500	255	N/A	
110	Arm—instrument swap	N/A	10	200	15	N/A	
110	MAHLI standard suite (25, 5, 2 cm standoff)	MAHLI target Fenrir borehole	8	18,000	8	N/A	
110	Arm—stow	N/A	20	500	45	N/A	
110	SuperCam power ON	Power on SuperCam	10	90	4	N/A	
111	SuperCam RMI image	RMI LD mosaic frame on target Nidavellir	1	2000	2	N/A	
111	SuperCam RMI image	RMI LD mosaic frame on target Nidavellir	1	2000	2	N/A	
111	SuperCam RMI image	RMI LD mosaic frame on target Nidavellir	1	2000	2	N/A	
111	SuperCam RMI image	RMI LD mosaic frame on target Nidavellir	1	2000	2	N/A	
111	SuperCam RMI image	RMI LD mosaic frame on target Nidavellir	1	2000	2	N/A	
111	SuperCam RMI image	RMI LD mosaic frame on target Nidavellir	1	2000	2	N/A	
111	SuperCam RMI image	RMI LD mosaic frame on target Gullveig	1	2000	2	N/A	
111	SuperCam RMI image	RMI LD mosaic frame on target Gullveig	1	2000	2	N/A	
111	SuperCam power OFF	Power off SuperCam	4	10	1	N/A	
111	MastCam mosaic—Z100	1 x 1 Z100 Doc of SuperCam LD RMI target Gullveig	3	4500	4	1	
111	MastCam mosaic—Z100	1 x 1 Z100 Doc of SuperCam LD RMI target Nidavellir	3	4500	4	1	
111	MastCam mosaic—Z100	7 x 1 (5 x 1 top, 2 x 1 bottom) mosaic on Jord	9	31,500	16	7	
111	MastCam image—clast survey	1 x 1 Z100 clast survey	3	6000	4	1	
111	Rover traverse—directed drive	Drive to eolian sampling location Jotunheimr	37.5	1100	44		11
111	NavCam panorama	NCAM PDI pano	25	20,000	25	N/A	
111	MastCam mosaic—work-space PDI	N/A	8	27,000	14	N/A	
111	MastCam image—clast survey	N/A	3	6000	4	N/A	
111	AEGIS analysis	Search for light-toned sand	5	1000	2		
111	SuperCam power ON	Power on SuperCam	10	90	4	N/A	
111	SuperCam VisIR 5 points	VisIR of AEGIS_111a	12	10,000	10	N/A	
111	SuperCam LIBS 5 points	LIBS of AEGIS_111a	12	10,000	10	N/A	
111	SuperCam RMI image	RMI of AEGIS_111a	1	2000	2	N/A	
111	SuperCam power OFF	Power off SuperCam	4	10	1	N/A	
111	MastCam mosaic—Z100	1 x 1 doc of SuperCam target AEGIS_111a	2	0	2	1	
112	Arm—unstow	N/A	20	500	45	N/A	
112	Arm—place on target	Target Valkyrie	10	500	20	N/A	

Table A1
(Continued)

Sol	Type	Description	Duration (minutes)	Data Usage (kB)	Energy Usage (Wh)	Frames	Drive Distance
112	MAHLI standard suite (25, 5, 2 cm standoff)	Full suite of dark sediment sample target Valkyrie	8	18,000	8	N/A	
112	Arm—instrument swap	N/A	10	200	15	N/A	
112	APXS—daytime short 45 minutes	Sample target Valkyrie	45	300	7	N/A	
112	Arm—instrument swap	N/A	10	200	15	N/A	
112	Sample acquisition	Sediment sample target Valkyrie	120	500	255	N/A	
112	Arm—move	N/A	10	500	30	N/A	
112	NavCam	NavCam L of postsampling target Valkyrie	5	50	1	1	
112	SuperCam power ON	Power on SuperCam	10	90	4	N/A	
113	SuperCam VisIR 5 points	VisIR of target Vali	12	10,000	10	N/A	
113	SuperCam LIBS 5 points	LIBS of target Vali	12	10,000	10	N/A	
113	SuperCam RMI image	RMI of target Vali	1	2000	2	N/A	
113	SuperCam VisIR 5 points	VisIR of target Vidar	12	10,000	10	N/A	
113	SuperCam LIBS 5 points	LIBS of target Vidar	12	10,000	10	N/A	
113	SuperCam RMI image	RMI of target Vidar	1	2000	2	N/A	
113	SuperCam power OFF	Power off SuperCam	4	10	1	N/A	
113	MastCam mosaic—Z100	1 x 1 Doc of Supercam Target Vidar	4	9000	6	2	
113	MastCam mosaic—Z100	1 x 1 Doc of Supercam Target Vali	4	9000	6	2	
113	MastCam mosaic—Z30	5 x 2 mosaic of target Vanaheimr	12	45,000	22	10	
113	Arm—stow	N/A	20	500	45		
113	Rover traverse—directed drive	Drive to depot location Alfheim	110	4000	160		40
113	NavCam panorama	NCAM PDI pano	25	20,000	25	N/A	
113	MastCam image—clast survey	N/A	3	6000	4	N/A	

Table A2
Rover LIBS and APXS Data, Including Weighted Averages for LIBS Data

Sol	Name	Al_2O_3 (%)	Al_2O_3 +/− (%)	CaO (%)	CaO +/−(%)	FeO (%)	FeO +/−(%)	K_2O (%)	K_2O +/− (%)	MgO (%)	MgO +/− (%)	MnO (%)	MnO +/− (%)	Na_2O (%)	Na_2O +/− (%)	O (%)	O +/− (%)	SiO_2 (%)	SiO_2 +/− (%)	TiO_2 (%)	TiO_2 +/− (%)	Total Alkali (%)	Total Alkali +/- (%)	Total
LIBS																								
101	Heimdall1	8.505	0.013	13.445	0.000	16.043	1.045	0.142	0.004	10.660	0.010	0.181	0.000	2.464	0.002	43.810	0.002	53.162	0.207	1.462	0.003			
101	Heimdall2	8.794	0.089	13.444	0.001	22.604	2.149	0.129	0.004	10.739	0.020	0.181	0.000	2.426	0.015	44.270	0.221	52.498	0.030	1.470	0.006			
101	Heimdall3	9.083	0.102	13.444	0.001	26.360	1.616	0.141	0.011	10.762	0.020	0.181	0.000	2.430	0.024	44.460	0.110	52.648	0.233	1.476	0.008			
101	Heimdall4	8.911	0.082	13.442	0.001	25.408	1.731	0.167	0.010	10.761	0.008	0.181	0.000	2.398	0.012	44.090	0.083	52.520	0.073	1.474	0.009			
101	Heimdall5	8.920	0.131	13.442	0.001	25.254	3.132	0.161	0.013	10.744	0.025	0.181	0.000	2.416	0.019	44.460	0.197	52.520	0.257	1.473	0.010			
101	Loki1	9.054	0.051	13.444	0.001	16.840	2.082	0.189	0.015	10.739	0.012	0.181	0.000	2.453	0.012	44.280	0.061	52.777	0.137	1.435	0.003			
101	Loki2	8.701	0.034	13.441	0.001	12.569	0.544	0.212	0.013	10.767	0.007	0.181	0.000	2.409	0.013	43.880	0.015	52.520	0.048	1.440	0.004			
101	Loki3	8.883	0.073	13.444	0.001	15.940	2.471	0.216	0.023	10.739	0.015	0.181	0.000	2.434	0.015	44.450	0.236	52.734	0.118	1.435	0.006			
101	Loki4	8.943	0.056	13.444	0.001	19.671	2.316	0.187	0.018	10.752	0.019	0.181	0.000	2.429	0.016	44.070	0.034	52.691	0.187	1.438	0.007			
101	Loki5	8.888	0.025	13.444	0.000	15.039	1.344	0.207	0.013	10.723	0.029	0.181	0.000	2.459	0.006	43.980	0.030	52.712	0.091	1.445	0.014			
101	Thor1	9.077	0.109	13.445	0.001	22.244	3.589	0.174	0.014	10.708	0.019	0.181	0.000	2.461	0.010	44.470	0.211	52.712	0.282	1.438	0.012			
101	Thor2	8.962	0.116	13.444	0.001	21.678	2.641	0.172	0.014	10.739	0.021	0.181	0.000	2.424	0.027	43.980	0.027	52.477	0.003	1.444	0.014			
101	Thor3	9.003	0.096	13.442	0.001	20.417	2.588	0.199	0.019	10.769	0.011	0.181	0.000	2.406	0.028	44.170	0.107	52.798	0.241	1.436	0.006			
101	Thor4	8.832	0.078	13.444	0.001	16.506	2.343	0.196	0.021	10.724	0.013	0.181	0.000	2.505	0.011	43.960	0.060	52.734	0.148	1.451	0.032			
101	Thor5	8.996	0.081	13.445	0.001	24.598	2.378	0.163	0.015	10.724	0.027	0.181	0.000	2.459	0.015	44.110	0.069	52.498	0.055	1.451	0.012			
102	Freya1	8.461	0.007	13.444	0.000	13.598	0.579	0.137	0.002	10.702	0.018	0.181	0.000	2.470	0.002	43.810	0.002	52.475	0.006	1.447	0.003			
102	Freya2	8.467	0.022	13.445	0.001	16.930	1.374	0.119	0.002	10.710	0.018	0.181	0.000	2.479	0.005	43.830	0.012	52.582	0.090	1.461	0.005			
102	Freya3	8.614	0.067	13.442	0.000	18.693	1.218	0.151	0.009	10.752	0.009	0.181	0.000	2.437	0.013	43.850	0.014	52.496	0.013	1.463	0.004			
102	Freya4	8.595	0.029	13.442	0.000	13.663	0.650	0.128	0.002	10.735	0.007	0.181	0.000	2.449	0.005	43.820	0.002	52.582	0.065	1.461	0.003			
102	Freya5	8.609	0.077	13.444	0.000	20.687	1.954	0.120	0.003	10.747	0.009	0.181	0.000	2.459	0.007	43.860	0.014	52.560	0.043	1.472	0.005			
102	Frigg1	9.020	0.128	13.442	0.001	22.823	3.034	0.196	0.020	10.750	0.014	0.181	0.000	2.424	0.017	44.320	0.194	52.496	0.033	1.446	0.016			
102	Frigg2	8.750	0.097	13.444	0.001	23.286	1.431	0.133	0.006	10.664	0.022	0.181	0.000	2.461	0.007	44.030	0.094	53.993	0.438	1.478	0.004			
102	Frigg3	9.002	0.064	13.442	0.001	26.116	1.357	0.170	0.009	10.704	0.015	0.181	0.000	2.425	0.012	44.380	0.097	53.822	1.007	1.490	0.004			
102	Frigg4	8.593	0.054	13.444	0.001	22.977	1.014	0.132	0.004	10.651	0.034	0.181	0.000	2.451	0.009	43.450	0.094	58.165	2.898	1.471	0.005			
102	Frigg5	8.862	0.096	13.444	0.001	24.096	1.113	0.146	0.006	10.651	0.029	0.181	0.000	2.422	0.015	43.340	0.102	53.715	0.425	1.481	0.005			
103	Baldur1	9.070	0.114	13.444	0.001	25.048	4.908	0.175	0.012	10.793	0.010	0.181	0.000	2.463	0.011	43.870	0.054	55.448	2.970	1.476	0.008			
103	Baldur2	8.909	0.027	13.441	0.000	11.774	0.978	0.181	0.010	10.699	0.011	0.181	0.000	2.436	0.009	43.820	0.011	58.165	2.264	1.461	0.004			
103	Baldur3	8.881	0.063	13.441	0.001	13.868	2.176	0.213	0.013	10.730	0.007	0.181	0.000	2.433	0.014	43.950	0.058	56.240	2.165	1.459	0.007			
103	Baldur4	8.943	0.058	13.441	0.001	18.886	2.866	0.208	0.018	10.772	0.008	0.181	0.000	2.416	0.016	43.910	0.026	52.667	0.103	1.468	0.007			
103	Baldur5	9.090	0.070	13.444	0.001	27.493	1.776	0.176	0.021	10.802	0.004	0.181	0.000	2.447	0.013	44.160	0.107	53.009	0.217	1.492	0.006			
103	Vili1	8.590	0.022	13.439	0.000	10.706	0.052	0.211	0.008	10.690	0.006	0.181	0.000	2.420	0.007	43.700	0.032	52.646	0.023	1.590	0.014			
103	Vili2	8.626	0.029	13.439	0.001	10.639	0.046	0.202	0.011	10.707	0.008	0.181	0.000	2.413	0.009	43.680	0.024	52.582	0.047	1.532	0.029			
103	Vili3	9.523	0.074	13.441	0.000	34.041	2.898	0.214	0.014	10.831	0.008	0.181	0.000	2.395	0.012	43.600	0.030	52.967	0.220	1.500	0.004			
103	Vili4	8.629	0.039	13.441	0.001	13.302	0.764	0.223	0.010	10.647	0.023	0.181	0.000	2.424	0.013	43.690	0.015	52.539	0.031	1.452	0.010			
103	Vili5	8.790	0.066	13.442	0.001	11.589	0.753	0.199	0.020	10.715	0.018	0.181	0.000	2.410	0.012	43.390	0.144	52.475	0.007	1.445	0.012			
104	Mjolnir1	8.716	0.029	13.441	0.001	10.683	0.093	0.199	0.006	10.712	0.009	0.181	0.000	2.401	0.005	43.520	0.059	52.582	0.054	1.528	0.025			
104	Mjolnir2	8.626	0.013	13.439	0.000	10.630	0.015	0.204	0.006	10.722	0.006	0.181	0.000	2.403	0.005	43.590	0.030	52.517	0.014	1.647	0.018			
104	Mjolnir3	8.601	0.016	13.441	0.000	10.744	0.045	0.185	0.009	10.697	0.009	0.181	0.000	2.408	0.006	43.730	0.012	52.517	0.018	1.572	0.014			
104	Mjolnir4	8.735	0.025	13.441	0.001	10.691	0.101	0.211	0.007	10.747	0.007	0.181	0.000	2.399	0.005	43.380	0.062	52.646	0.053	1.585	0.030			
104	Mjolnir5	8.729	0.027	13.439	0.001	10.628	0.027	0.207	0.010	10.699	0.010	0.181	0.000	2.394	0.007	43.610	0.037	52.539	0.074	1.526	0.023			
107	Muspelheim1	8.837	0.078	13.442	0.001	19.966	1.789	0.130	0.005	10.760	0.007	0.181	0.000	2.441	0.012	43.620	0.028	52.517	0.034	1.465	0.005			
107	Muspelheim2	8.663	0.136	13.445	0.001	22.681	1.800	0.123	0.003	10.715	0.011	0.181	0.000	2.474	0.007	43.380	0.139	54.806	1.178	1.480	0.004			
107	Muspelheim3	8.558	0.063	13.444	0.001	18.024	2.145	0.121	0.002	10.720	0.017	0.181	0.000	2.474	0.003	43.640	0.062	53.673	0.827	1.472	0.005			
107	Muspelheim5	8.867	0.077	13.441	0.001	23.363	1.187	0.149	0.010	10.667	0.024	0.181	0.000	2.478	0.004	43.290	0.114	133.251	57.737	1.479	0.003			
107	Muspelheim4	8.661	0.039	13.441	0.000	17.612	1.373	0.149	0.005	10.745	0.011	0.181	0.000	2.425	0.012	43.730	0.012	53.566	0.796	1.470	0.004			
107	Niflheim1	8.576	0.103	13.441	0.001	22.359	1.033	0.181	0.016	10.788	0.004	0.181	0.000	2.429	0.016	43.510	0.087	52.667	0.189	1.476	0.004			
107	Niflheim2	8.671	0.066	13.439	0.001	17.136	2.252	0.146	0.006	10.777	0.008	0.181	0.000	2.421	0.014	43.690	0.029	52.496	0.026	1.451	0.010			
107	Niflheim3	8.694	0.058	13.439	0.001	17.754	1.819	0.230	0.014	10.763	0.009	0.181	0.000	2.428	0.010	43.400	0.104	52.753	0.298	1.452	0.005			
107	Niflheim4	8.546	0.032	13.441	0.001	14.563	0.932	0.169	0.015	10.717	0.013	0.181	0.000	2.447	0.010	43.680	0.037	52.517	0.031	1.455	0.003			
107	Niflheim5	8.824	0.113	13.438	0.001	22.347	1.785	0.218	0.014	10.750	0.011	0.181	0.000	2.391	0.018	42.410	0.413	54.250	0.948	1.475	0.006			
108	Aegis_108A1	8.525	0.026	13.441	0.001	11.387	0.597	0.158	0.010	10.672	0.030	0.181	0.000	2.444	0.015	43.760	0.011	52.881	0.387	1.442	0.007			
108	Aegis_108A2	8.457	0.001	13.444	0.000	10.659	0.054	0.152	0.004	10.599	0.018	0.181	0.000	2.475	0.003	43.770	0.003	52.496	0.008	1.435	0.001			
108	Aegis_108A3	8.461	0.002	13.444	0.000	10.720	0.107	0.132	0.004	10.664	0.016	0.181	0.000	2.470	0.002	43.780	0.002	52.496	0.006	1.434	0.002			
108	Aegis_108A4	8.499	0.025	13.444	0.000	10.692	0.124	0.163	0.008	10.629	0.027	0.181	0.000	2.461	0.007	43.770	0.003	53.587	0.367	1.437	0.003			

Table A2
(Continued)

Sol	Name	Al_2O_3 (%)	Al_2O_3 +/− (%)	CaO (%)	CaO +/−(%)	FeO (%)	FeO +/−(%)	K_2O (%)	K_2O +/− (%)	MgO (%)	MgO +/− (%)	MnO (%)	MnO +/− (%)	Na_2O (%)	Na_2O +/− (%)	O (%)	O +/− (%)	SiO_2 (%)	SiO_2 +/− (%)	TiO_2 (%)	TiO_2 +/− (%)	Total Alkali (%)	Total Alkali +/- (%)	Total
108	Aegis_108A5	8.631	0.067	13.441	0.001	11.674	0.675	0.206	0.024	10.685	0.027	0.181	0.000	2.414	0.018	43.730	0.029	54.870	1.369	1.440	0.006			
108	hel1	8.516	0.016	13.442	0.000	10.868	0.222	0.222	0.007	10.674	0.007	0.181	0.000	2.519	0.009	43.780	0.005	52.603	0.036	1.820	0.047			
108	h2	8.586	0.035	13.442	0.001	10.737	0.146	0.222	0.008	10.674	0.014	0.181	0.000	2.470	0.009	43.710	0.028	52.646	0.078	1.645	0.051			
108	h3	9.024	0.042	13.446	0.001	21.755	2.162	0.205	0.018	10.735	0.013	0.181	0.000	2.463	0.011	43.240	0.167	52.496	0.027	1.446	0.009			
108	h4	8.614	0.017	13.439	0.000	11.252	0.174	0.265	0.004	10.705	0.006	0.181	0.000	2.506	0.014	43.760	0.020	52.795	0.087	1.683	0.027			
108	h5	8.686	0.041	13.442	0.001	11.851	0.850	0.236	0.016	10.714	0.014	0.181	0.000	2.449	0.008	43.630	0.040	52.688	0.118	1.527	0.052			
109	aegir1	8.869	0.075	13.441	0.001	20.069	2.363	0.174	0.013	10.740	0.010	0.181	0.000	2.416	0.013	43.730	0.024	52.560	0.102	1.467	0.006			
109	aegir2	8.624	0.035	13.441	0.000	10.720	0.332	0.201	0.011	10.664	0.027	0.181	0.000	2.457	0.009	43.780	0.016	52.539	0.063	1.438	0.007			
109	aegir3	8.971	0.048	13.442	0.001	14.229	1.006	0.302	0.017	10.740	0.041	0.181	0.000	2.434	0.008	43.520	0.119	53.159	0.588	1.439	0.004			
109	aegir4	8.497	0.016	13.444	0.001	11.011	0.148	0.163	0.006	10.636	0.020	0.181	0.000	2.453	0.006	43.780	0.004	52.539	0.048	1.434	0.001			
109	aegir5	8.575	0.029	13.441	0.001	10.740	0.195	0.179	0.007	10.669	0.021	0.181	0.000	2.425	0.014	43.760	0.018	52.496	0.012	1.434	0.001			
109	fenrir1	8.457	0.003	13.446	0.001	10.634	0.024	0.137	0.002	10.541	0.027	0.181	0.000	2.479	0.003	43.780	0.002	53.651	0.634	1.439	0.003			
109	fenrir2	8.548	0.044	13.444	0.000	10.628	0.042	0.197	0.007	10.677	0.020	0.181	0.000	2.494	0.005	43.720	0.020	52.582	0.043	1.443	0.008			
109	fenrir3	8.605	0.025	13.441	0.000	13.084	0.576	0.200	0.006	10.679	0.035	0.181	0.000	2.428	0.004	43.760	0.009	52.539	0.042	1.449	0.003			
110	jord1	8.920	0.061	13.441	0.001	17.188	1.976	0.213	0.018	10.740	0.009	0.181	0.000	2.401	0.014	43.760	0.011	52.646	0.153	1.465	0.006			
110	jord2	9.623	0.021	13.442	0.000	63.592	2.561	0.117	0.001	10.858	0.005	0.181	0.000	2.495	0.002	43.720	0.025	52.496	0.027	1.521	0.004			
110	jord3	8.883	0.092	13.441	0.001	14.525	2.495	0.213	0.014	10.712	0.019	0.181	0.000	2.406	0.019	43.760	0.039	52.539	0.043	1.442	0.008			
110	jord4	9.003	0.084	13.442	0.000	19.786	2.781	0.147	0.009	10.808	0.007	0.181	0.000	2.436	0.006	43.790	0.048	53.181	0.315	1.462	0.009			
110	jord5	8.760	0.045	13.441	0.001	14.447	0.863	0.220	0.014	10.702	0.018	0.181	0.000	2.417	0.014	43.800	0.010	52.496	0.040	1.449	0.004			
110	fenrir1	9.000	0.064	13.444	0.001	16.763	1.939	0.172	0.015	10.739	0.021	0.181	0.000	2.440	0.014	42.370	0.257	52.667	0.201	1.434	0.002			
110	fenrir2	8.712	0.029	13.441	0.001	11.478	0.688	0.217	0.015	10.714	0.032	0.181	0.000	2.406	0.009	43.630	0.079	52.517	0.085	1.527	0.050			
110	fenrir3	8.669	0.027	13.439	0.001	11.366	0.472	0.233	0.013	10.775	0.008	0.181	0.000	2.395	0.012	43.590	0.095	52.646	0.127	1.545	0.044			
110	fenrir4	8.864	0.048	13.439	0.001	11.981	0.906	0.240	0.017	10.719	0.025	0.181	0.000	2.390	0.013	43.140	0.273	52.539	0.269	1.502	0.035			
110	fenrir5	8.656	0.014	13.439	0.000	10.805	0.100	0.203	0.004	10.740	0.009	0.181	0.000	2.394	0.004	43.640	0.067	52.603	0.054	1.627	0.028			
111	aegis1	8.463	0.008	13.444	0.000	20.005	0.841	0.138	0.003	10.656	0.006	0.181	0.000	2.470	0.003	43.750	0.007	56.026	0.658	1.466	0.003			
111	aegis2	8.544	0.032	13.445	0.000	20.610	0.906	0.126	0.002	10.624	0.014	0.181	0.000	2.479	0.003	43.700	0.019	54.678	0.576	1.472	0.003			
111	aegis3	8.478	0.011	13.444	0.000	20.764	0.507	0.127	0.003	10.649	0.012	0.181	0.000	2.479	0.002	43.740	0.006	53.951	0.587	1.471	0.001			
111	aegis4	8.457	0.000	13.444	0.000	19.272	0.506	0.128	0.002	10.669	0.008	0.181	0.000	2.484	0.001	43.750	0.008	54.443	0.527	1.467	0.002			
111	aegis5	8.461	0.007	13.445	0.000	18.590	0.608	0.127	0.002	10.621	0.008	0.181	0.000	2.486	0.001	43.750	0.011	55.234	0.905	1.462	0.004			
113	vali1	8.469	0.015	13.445	0.000	17.458	0.835	0.125	0.002	10.543	0.009	0.181	0.000	2.480	0.004	43.730	0.008	57.052	1.239	1.451	0.003			
113	vali2	8.484	0.010	13.446	0.000	16.750	0.546	0.120	0.001	10.568	0.014	0.181	0.000	2.488	0.002	43.780	0.001	58.486	0.963	1.446	0.002			
113	vali3	8.480	0.008	13.446	0.000	17.972	0.333	0.117	0.001	10.510	0.020	0.181	0.000	2.494	0.001	43.770	0.003	60.924	1.552	1.453	0.002			
113	vali4	8.533	0.036	13.445	0.000	19.259	0.791	0.119	0.001	10.609	0.017	0.181	0.000	2.482	0.002	43.740	0.008	53.886	0.593	1.461	0.004			
113	vali5	8.601	0.067	13.445	0.001	21.394	1.096	0.125	0.005	10.596	0.016	0.181	0.000	2.465	0.009	43.670	0.028	54.036	0.754	1.463	0.004			
113	vidar1	8.968	0.074	13.442	0.001	24.688	1.433	0.178	0.011	10.763	0.009	0.181	0.000	2.371	0.018	43.030	0.155	52.603	0.102	1.477	0.005			
113	vidar2	8.544	0.051	13.441	0.001	18.088	1.268	0.156	0.018	10.700	0.032	0.181	0.000	2.416	0.016	43.440	0.186	52.603	0.103	1.436	0.004			
113	vidar3	8.520	0.025	13.442	0.000	17.201	0.677	0.172	0.010	10.699	0.012	0.181	0.000	2.449	0.007	43.700	0.016	52.517	0.032	1.436	0.002			
113	vidar4	8.697	0.078	13.444	0.000	20.867	1.101	0.141	0.005	10.737	0.011	0.181	0.000	2.434	0.009	43.360	0.126	52.539	0.056	1.457	0.007			
113	vidar5	8.599	0.067	13.444	0.001	19.555	0.924	0.129	0.004	10.697	0.013	0.181	0.000	2.440	0.011	43.490	0.053	52.496	0.022	1.450	0.007			
APXS																								
103	Mjolnir	8.907	0.050	13.444	0.001	13.701	1.263	0.184	0.014	10.692	0.014	0.181	0.000	2.416	0.013	43.040	0.133	52.624	0.217	1.434	0.002			
106	Njord	8.631	0.109	13.442	0.001	25.254	1.092	0.118	0.004	10.778	0.007	0.181	0.000	2.434	0.019	43.380	0.191	52.560	0.194	1.481	0.002			
109	fenrir	8.832	0.083	13.442	0.001	14.216	1.655	0.195	0.016	10.773	0.010	0.181	0.000	2.409	0.014	42.510	0.264	52.496	0.016	1.440	0.010			
112	valkyrie	8.514	0.033	13.444	0.000	21.240	1.270	0.138	0.004	10.647	0.023	0.181	0.000	2.459	0.006	43.590	0.068	53.138	0.426	1.460	0.004			
LIBS Weighted Average																								
Name	Category																							
Heimdall1	L and D Sand	8.534	0.013	13.444	0.000	20.878	0.716	0.139	0.002	10.725	0.006	0.181	0.000	2.462	0.002	43.810	0.002	52.515	0.027	1.466	0.003	2.601	0.003	110.344
Loki1	Old Lava	8.864	0.017	13.443	0.000	13.506	0.471	0.202	0.007	10.757	0.005	0.181	0.000	2.448	0.005	43.940	0.012	52.601	0.038	1.437	0.002	2.650	0.008	103.438
Thor1	Old Lava	8.959	0.041	13.444	0.000	20.896	1.171	0.177	0.007	10.743	0.007	0.181	0.000	2.471	0.006	44.005	0.022	52.477	0.003	1.440	0.005	2.648	0.009	110.787
Freya1	L and D Sand	8.470	0.006	13.443	0.000	14.656	0.383	0.127	0.001	10.739	0.004	0.181	0.000	2.467	0.002	43.816	0.001	52.481	0.006	1.458	0.002	2.593	0.002	104.022
Frigg1	D Sand	8.790	0.034	13.443	0.000	23.916	0.585	0.140	0.003	10.706	0.009	0.181	0.000	2.447	0.004	43.840	0.047	52.514	0.033	1.480	0.002	2.588	0.005	113.619

Table A2
(Continued)

Sol	Name	Al_2O_3 (%)	Al_2O_3 +/− (%)	CaO (%)	CaO +/−(%)	FeO (%)	FeO +/−(%)	K_2O (%)	K_2O +/− (%)	MgO (%)	MgO +/− (%)	MnO (%)	MnO +/− (%)	Na_2O (%)	Na_2O +/− (%)	O (%)	O +/− (%)	SiO_2 (%)	SiO_2 +/− (%)	TiO_2 (%)	TiO_2 +/− (%)	Total Alkali (%)	Total Alkali +/- (%)	Total
Baldur1	Old Lava	8.933	0.021	13.442	0.000	15.715	0.759	0.189	0.006	10.775	0.003	0.181	0.000	2.442	0.005	43.840	0.010	52.748	0.092	1.469	0.002	2.631	0.008	105.893
Vili1	Old Lava	8.655	0.015	13.440	0.000	10.679	0.034	0.212	0.005	10.727	0.004	0.181	0.000	2.414	0.004	43.675	0.011	52.494	0.006	1.496	0.004	2.626	0.007	100.297
Mjolnir1	Old Lava	8.649	0.009	13.440	0.000	10.640	0.012	0.202	0.003	10.720	0.004	0.181	0.000	2.401	0.002	43.686	0.011	52.525	0.010	1.579	0.009	2.603	0.004	100.338
Muspelheim1	L Sand	8.690	0.028	13.442	0.000	20.726	0.694	0.126	0.001	10.742	0.005	0.181	0.000	2.472	0.002	43.705	0.011	52.523	0.034	1.475	0.002	2.598	0.003	110.377
Niflheim1	D Sand	8.604	0.025	13.439	0.000	18.430	0.587	0.167	0.005	10.775	0.003	0.181	0.000	2.429	0.006	43.660	0.021	52.509	0.020	1.464	0.002	2.596	0.007	107.998
Aegis_108A1	New Lava	8.458	0.001	13.443	0.000	10.682	0.044	0.146	0.002	10.644	0.010	0.181	0.000	2.470	0.002	43.774	0.001	52.496	0.005	1.435	0.001	2.616	0.003	99.956
Hel1	old lava	8.602	0.011	13.441	0.000	10.969	0.099	0.248	0.003	10.696	0.004	0.181	0.000	2.478	0.004	43.775	0.004	52.561	0.020	1.488	0.008	2.726	0.005	100.664
Aegir1	New Lava	8.568	0.012	13.441	0.000	10.951	0.110	0.182	0.004	10.709	0.008	0.181	0.000	2.444	0.004	43.778	0.003	52.500	0.011	1.434	0.000	2.626	0.005	100.410
Fenrir1 no abrade	New Lava	8.461	0.003	13.442	0.000	10.636	0.021	0.151	0.002	10.639	0.014	0.181	0.000	2.464	0.002	43.779	0.002	52.562	0.030	1.444	0.002	2.615	0.003	99.979
Jord1	New Lava	9.389	0.017	13.442	0.000	18.809	0.700	0.120	0.001	10.811	0.004	0.181	0.000	2.482	0.002	43.777	0.007	52.510	0.019	1.476	0.002	2.602	0.003	109.219
Fenrir1 abrade	New Lava	8.686	0.011	13.440	0.000	10.870	0.096	0.206	0.004	10.755	0.006	0.181	0.000	2.398	0.003	43.576	0.044	52.588	0.041	1.436	0.002	2.605	0.005	100.560
Aegis1 111a	D sand	8.457	0.000	13.444	0.000	19.776	0.276	0.128	0.001	10.647	0.004	0.181	0.000	2.483	0.001	43.745	0.004	54.742	0.277	1.469	0.001	2.611	0.001	111.328
Vali1	D Sand	8.482	0.006	13.445	0.000	17.977	0.248	0.120	0.001	10.560	0.006	0.181	0.000	2.491	0.001	43.776	0.001	55.399	0.385	1.452	0.001	2.611	0.001	110.107
Vidar1	D Sand	8.574	0.020	13.443	0.000	19.089	0.435	0.141	0.003	10.730	0.006	0.181	0.000	2.436	0.004	43.672	0.015	52.511	0.017	1.443	0.002	2.577	0.005	108.548

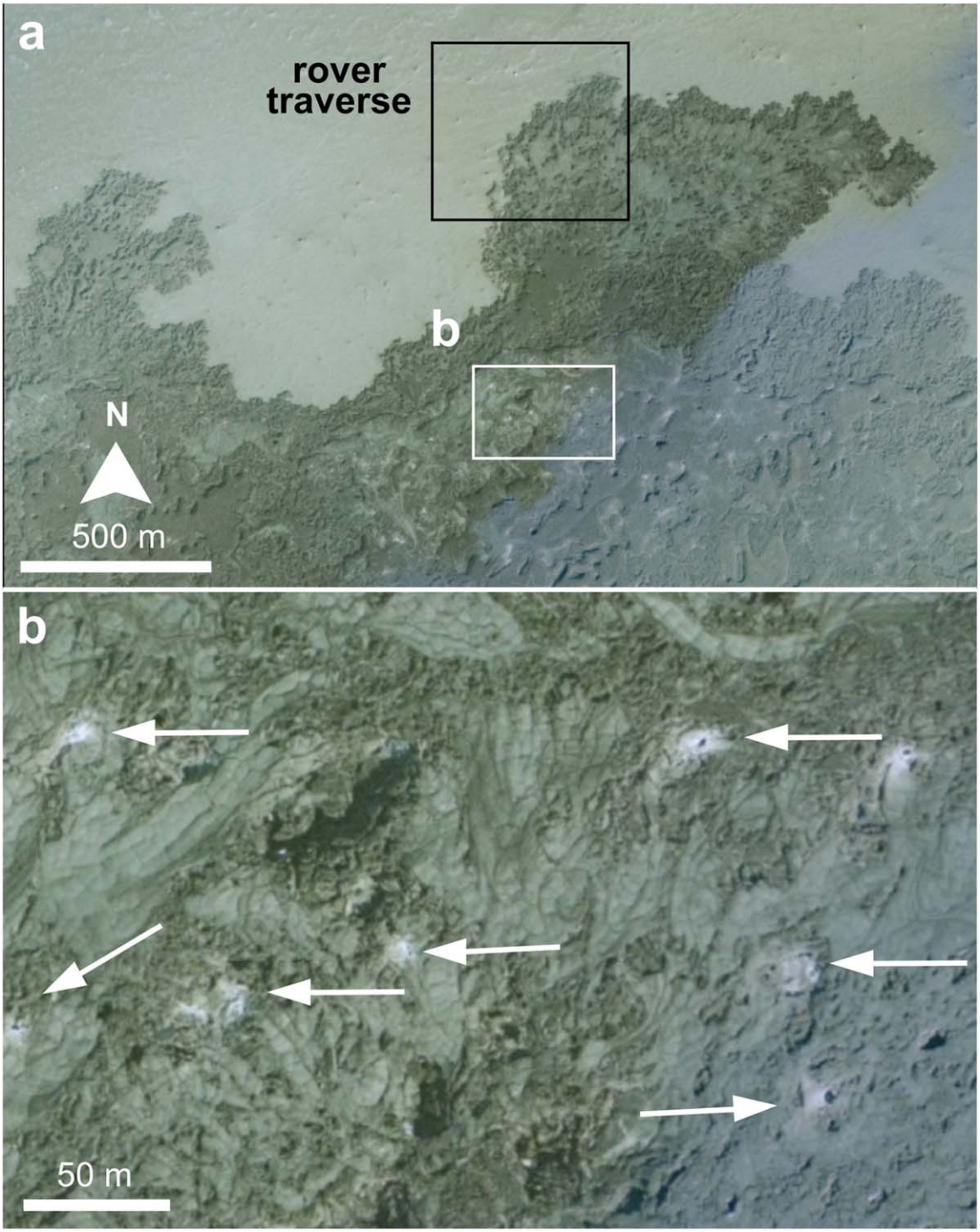

Figure A1. Examples of light-toned zones of alteration identified from remotely sensed images. The black box in (a) indicates the area of the 2022 rover traverse for comparison. The white box in (a) indicates the location of (b). White arrows in (b) indicate light-toned zones of alteration. The base map is sourced from Loftmyndir Einkahlutafélag. (50 cm pixel^{-1}).

ORCID iDs

Samantha Gwizd https://orcid.org/0000-0001-5818-9123
Brett B. Carr https://orcid.org/0000-0002-1033-3082

References

Alibay, F., Koch, J., Verma, V., et al. 2022, in 2022 IEEE Aerospace Conf. (Piscataway, NJ: IEEE), 1
Allwood, A. C., Wade, L. A., Foote, M. C., et al. 2020, SSRv, 216, 134
Arvidson, R. E., Poulet, F., Morris, R. V., et al. 2006, JGRE, 111, E12S08
Babechuk, M. G., Widdowson, M., & Kamber, B. S. 2014, ChGeo, 363, 56
Balaram, B., Canham, T., Duncan, C., et al. 2018, in 2018 AIAA Atmospheric Flight Mechanics Conf. (Reston, VA: AIAA), 1
Bapst, J., Parker, T. J., Balaram, J., et al. 2021, BAAS, 53, 361
Barnes, J. W., Turtle, E. P., Trainer, M. G., et al. 2021, PSJ, 2, 130
Basu, U., Moersch, J., Hamilton, C. W., et al. 2022, LPSC, 53, 2362
Bell, J. F., III, Godber, A., McNair, S., et al. 2017, E&SS, 4, 396
Bell, J. F., Maki, J. N., Mehall, G. L., et al. 2021, SSRv, 217, 24
Bhartia, R., Beegle, L. W., DeFlores, L., et al. 2021, SSRv, 217, 58
Blake, D., Vaniman, D., Achilles, C., et al. 2012, SSRv, 170, 341

Bonnefoy, L. E., Hamilton, C. W., Scheidt, S. P., et al. 2019, JVGR, 387, 106652
Bonny, E., Thordarson, T., Wright, R., Höskuldsson, A., & Jónsdóttir, I. 2018, JGRB, 123, 5412
Cady, S. L., & Farmer, J. D. 1996, in Ciba Foundation Symp. 202—Evolution of Hydrothermal Ecosystems on Earth (And Mars?), ed. G. R. Bock & J. A. Goode (New York: Wiley), 150
Caravaca, G., Mangold, N., Dehouck, E., et al. 2022, JGRE, 127, e07093
Carr, B. B., Varnam, M., Hadland, N., et al. 2024, PSJ, submitted
Chattopadhyay, D., Mishkin, A., Allbaugh, A., et al. 2014, in SpaceOps 2014 Conf. (Reston, VA: AIAA), 1
Crisp, J. A., Adler, M., Matijevic, J. R., et al. 2003, JGRE, 108, 8061
Davis, K., Herman, J., Maksymuk, et al. 2012, in 41st Aerospace Mechanisms Symp. (Pasadena, CA: JPL, Caltech), 279, https://www.esmats.eu/amspapers/pastpapers/pdfs/2012/davis.pdf
Duhamel, S., Hamilton, C. W., Pálsson, S., & Björnsdóttir, S. H. 2022, AsBio, 22, 1176
Dundas, C. M., Keszthelyi, L., Lev, et al. 2020, JVGR, 408, 107100
Dutta, S., & Way, D. W. 2017, in AIAA Atmospheric Flight Mechanics Conf. (Reston, VA: AIAA), 0245
Edgett, K. S., Yingst, R. A., Ravine, M. A., et al. 2012, SSRv, 170, 259
Edwards, C. D., Bell, D. J., Gladden, R. E., et al. 2013, in 2013 IEEE Aerospace Conf. (Piscataway, NJ: IEEE), 1
Farley, K. A., Stack, K. M., Shuster, D. L., et al. 2022, Sci, 377, eabo2196
Farley, K. A., Williford, K. H., Stack, K. M., et al. 2020, SSRv, 216, 142
Farmer, J. D., & Des Marais, D. J. 1999, JGR, 104, 26977
Francis, R., Estlin, T., Doran, G., et al. 2017, Science Robotics, 2, eaan4582
Gaines, D., Anderson, R., Doran, G., et al. 2016, in Proc. 4th Workshop on Planning and Robotics (PlanRob), 115
Gellert, R., Clark, B. C., III & MSL and MER Science Teams 2015, Eleme, 11, 39
Golombek, M. P., Anderson, R. C., Barnes, J. R., et al. 1999, JGR, 104, 8523
Golombek, M., Grant, J., Kipp, D., et al. 2012, SSRv, 170, 641
Golombek, M., Williams, N., Grip, H., et al. 2022, COSPAR Scientific Assembly, 44, B4.2–0005-22
Grant, J. A., Golombek, M. P., Wilson, S. A., et al. 2018, P&SS, 164, 106
Grotzinger, J. P., Crisp, J., Vasavada, A. R., et al. 2012, SSRv, 170, 5
Grotzinger, J. P., Gupta, S., Malin, M. C., et al. 2015, Sci, 350, aac7575
Grotzinger, J. P., Sumner, D. Y., Kah, L. C., et al. 2014, Sci, 343, 1242777
Gudmundsson, M. T., Jónsdóttir, K., Hooper, A., et al. 2016, Sci, 353, aaf8988
Hadland, N., Hamilton, C. W., & Duhamel, S. 2024, ComEE, 5, 114
Hamilton, C. W., Voigt, J. R. C., Zanetti, M., et al. 2023, LPSC, 54, 3010
Hamilton, C. W., Scheidt, S. P., Sori, M. M., et al. 2020, JGRE, 125, e05975
Hartley, M. E., & Thordarson, T. 2013, GGG, 14, 2286
Hays, L. E., Graham, H. V., Des Marais, D. J., et al. 2017, AsBio, 17, 363
Indyk, S., Spring, J., Ford, S., Luczek, K., & Paulsen, G. 2018, in 2018 SpaceOps Conf. (Reston, VA: AIAA), 2322
Jacob, S. R., Wellington, D. F., Bell, J. F., et al. 2020, JGRE, 125, e06290
James, M. R., Carr, B., D'Arcy, F., et al. 2020, Volcanica, 3, 67
Johnson, W., Withrow-Maser, S., Young, L., et al. 2020, Mars Science Helicopter Conceptual Design. NASA Technical Rep. ARC-E-DAA-TN78199, NASA Ames Research Center
Langley, C., Chappell, L., Ratti, J., et al. 2012, in Proc. Int. Symp. on Artificial Intelligence Robotics and Automation in Space (Noordwijk: ESA), http://asrl.utias.utoronto.ca/~tdb/bib/langley_isairas12.pdf
Mahaffy, P. R., Webster, C. R., Cabane, M., et al. 2012, SSRv, 170, 401
Maki, J. N., Gruel, D., McKinney, C., et al. 2020, SSRv, 216, 137
Maki, J., Thiessen, D., Pourangi, A., et al. 2012, SSRv, 170, 77
Malin, M. C., Bell, J. F., III, Cantor, B. A., et al. 2007, JGRE, 112, E05S04
Mangold, N., Gupta, S., Gasnault, O., et al. 2021, Sci, 374, 711
Maurice, S., Wiens, R. C., Bernardi, P., et al. 2021, SSRv, 217, 47
McEwen, A. S., Eliason, E. M., Bergstrom, J. W., et al. 2007, JGRE, 112, E05S02
McLennan, S. M., Grotzinger, J. P., Hurowitz, J. A., & Tosca, N. J. 2019, AREPS, 47, 91
MEPAG 2020, in Mars Scientific Goals, Objectives, Investigations, and Priorities, ed. D. Banfield, https://mepag.jpl.nasa.gov/reports/MEPAGGoals_2020_MainText_Final.pdf
Milkovich, S. M., Stack, K. M., Sun, V. Z., et al. 2022, in 2022 IEEE Aerospace Conf. (AERO) (Piscataway, NJ: IEEE), 1
Moeller, R. C., Jandura, L., Rosette, K., et al. 2021, SSRv, 217, 5
Nachon, M., Clegg, S. M., Mangold, N., et al. 2014, JGRE, 119, 1991
Olsson-Francis, K., Doran, P. T., Ilyin, V., et al. 2023, LSSR, 36, 27
Pedersen, G. B. M., Höskuldsson, A., Dürig, T., et al. 2017, JVGR, 340, 155
Rampe, E. B., Blake, D. F., Bristow, T. F., et al. 2020, ChEG, 80, 125605
Rivera-Hernández, F., Sumner, D. Y., Mangold, N., et al. 2020, JGRE, 125, e06230
Rowland, S. K., & Walker, G. P. L. 1987, BVol, 49, 631
Scheller, E. L., Razzell Hollis, J., Cardarelli, E. L., et al. 2022, Sci, 378, 1105
Scheidt, S. P., & Hamilton, C. W. 2019, Unmanned Aerial System (UAS)-derived Orthoimage Mosaics and Digital Terrain Models of the North-eastern Portion of the 2014–2015 Holuhraun Lava Flow-field, Iceland: Data Acquired from 2015 to 2018. University of Arizona, Department of Planetary Sciences, Lunar and Planetary Laboratory, doi:10.25422/azu.data.c.5214641.v2
Simon, J. I., Hickman-Lewis, K., Cohen, B. A., et al. 2023, JGRE, 128, e2022JE007474
Squyres, S. W., Arvidson, R. E., Bollen, D., et al. 2006, JGRE, 111, E12S12
Stack, K. M., Grotzinger, J. P., Lamb, M. P., et al. 2019, Sedimentology, 66, 1768
Sullivan, R., Anderson, R., Biesiadecki, J., Bond, T., & Stewart, H. 2011, JGRE, 116, E02006
Sun, V., Sholes, S., Pyrzak, G., et al. 2024, in 2024 IEEE Aerospace Conf. (Piscataway, NJ: IEEE), 1
Sutton, S. S., Chojnacki, M., McEwen, A. S., et al. 2022, RemS, 14, 2403
Udry, A., Ostwald, A., Sautter, V., et al. 2023, JGRE, 128, e2022JE007440
Vasavada, A. R. 2022, SSRv, 218, 14
Verma, V., Maimone, M., Del Sesto, T., et al. 2024, in 2024 IEEE Aerospace Conf. (Piscataway, NJ: IEEE), 1
Voigt, J. R., Hamilton, C. W., Scheidt, S. P., et al. 2021a, JVGR, 419, 107278
Voigt, J. R., Hamilton, C. W., Steinbrügge, G., & Scheidt, S. P. 2021b, BVol, 83, 82
Voigt, J. R., Hamilton, C. W., Steinbrügge, G., et al. 2023, JGRE, 128, e2023JE007947
Walker, G. P. L. 2009, in Studies in Volcanology: The Legacy of George Walker, ed. T. Thordarson et al. (McLean, VA: GeoScienceWorld), 17
Wiens, R. C., Maurice, S., Barraclough, B., et al. 2012, SSRv, 170, 167
Williams, R. M., Grotzinger, J. P., Dietrich, W. E., et al. 2013, Sci, 340, 1068
Yingst, R. A., Cohen, B. A., Hynek, B., et al. 2014, AcAau, 99, 24
Yingst, R. A., Kah, L. C., Palucis, M., et al. 2013, JGRE, 118, 2361